JCI The Journal of Clinical Investigation

PIK3CA inhibition in models of proliferative glomerulonephritis and lupus nephritis

Junna Yamaguchi, … , Fabiola Terzi, Guillaume Canaud

J Clin Invest. 2024. https://doi.org/10.1172/JCI176402.

Research In-Press Preview Nephrology

Graphical abstract

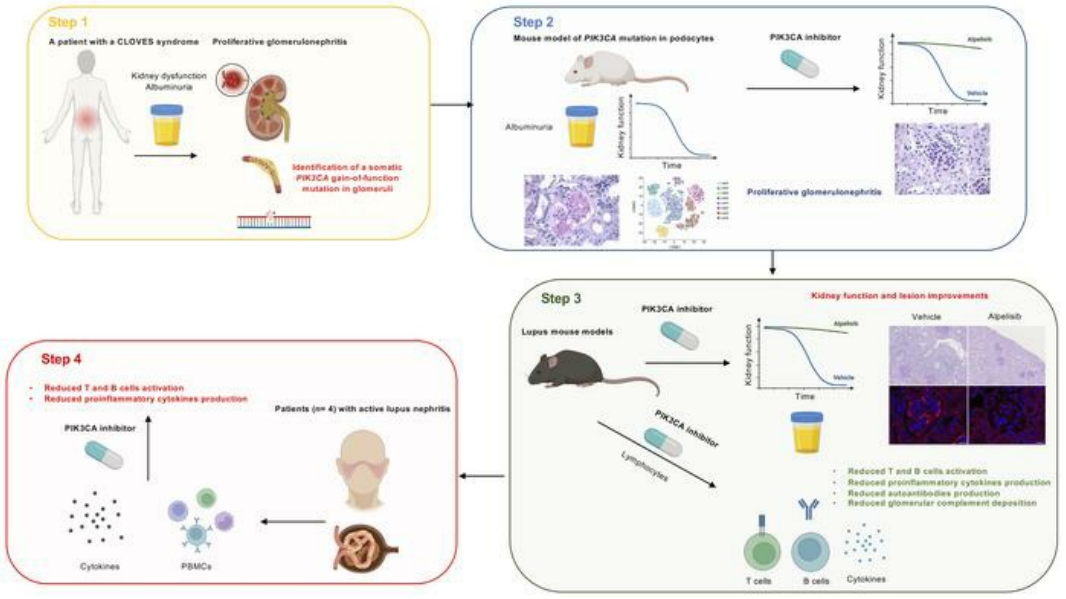

Find the latest version:

https://jci.me/176402/pdf

PIK3CA inhibition in models of proliferative glomerulonephritis and lupus nephritis

Junna Yamaguchi (MD, PhD)[1,2,3], Pierre Isnard (MD, PhD)[1,3,4], Noémie Robil (PhD)[5], Pierre de la Grange (PhD)[5], Clément Hoguin (BSc)[1,2,3], Alain Schmitt (BSc)[6], Aurélie Humel (MD)[7], Jérôme Megret (PhD)[8], Nicolas Goudin (PhD)[8], Marine Luka (PhD)[9,10], Mickael Menager (PhD)[9,10], Cécile Masson (PhD)[11], Mohammed Zarhrate (BSc)[12], Christine Bôle-Feysot (PhD)[12], Michalina Janiszewska (MD, PhD)[13], Kornelia Polyak (MD, PhD)[14,15], Julien Dairou (PhD)[1,16], Sara Baldassari (PhD)[17], Stéphanie Baulac (PhD)[17], Christine Broissand (PhD)[18], Christophe Legendre (MD, PhD)[1,3,7], Fabiola Terzi (MD, PhD)[3], Guillaume Canaud (MD, PhD)[1,2,3]

1 Université Paris Cité, Paris, France
2 Unité de Médecine Translationnelle et Thérapies Ciblées, Hôpital Necker-Enfants Malades, AP-HP, Paris, France
3 INSERM U1151, Institut Necker-Enfants Malades, Paris, France
4 Service d'Anatomie pathologique, Hôpital Necker-Enfants Malades, AP-HP, Paris, France
5 Genosplice Technology, Paris Biotech Santé, Paris, France
6 Institut Cochin, Paris, France
7 Service de Néphrologie, Transplantation Adultes, Hôpital Necker-Enfants Malades, AP-HP, Paris, France
8 Structure Fédérative de Recherche Necker, INSERM US24,-CNRS UAR 3633, Institut Necker-Enfants Malades, Paris, France
9 Inflammatory Responses and Transcriptomic Networks in Diseases, Institut Imagine, Paris, France
10 INSERM U1163, Institut Imagine, Paris, France
11 Bioinformatics Platform, Structure Fédérative de Recherche Necker, INSERM UMR1163, Université de Paris, Imagine Institute, Paris, France
12 Plateforme Génomique, INSERM U1163, Institut Imagine, Paris, France
13 Department of Molecular Medicine, The Herbert Wertheim UF Scripps Institute for Biomedical Innovation and Technologies, Jupiter, FL, USA
14 Department of Medical Oncology, Dana-Farber Cancer Institute, Boston, USA
15 Department of Medicine, Harvard Medical School, Boston, USA
16 Laboratoire de Chimie et Biologie Pharmacologiques et Toxicologiques, Paris, France
17 Sorbonne Université, Institut du Cerveau - Paris Brain Institute - ICM, Inserm, CNRS, Hôpital de la Pitié Salpêtrière, 75013 Paris, France
18 Pharmacie, Hôpital Necker-Enfants Malades, AP-HP, Paris, France

† Corresponding author:
Prof. Guillaume Canaud
Université Paris Cité
Unité de médecine translationnelle et thérapies ciblées, Hôpital Necker-Enfants Malades, AP-HP, Paris, France
Institut National de la Santé et de la Recherche Médicale U1151
149 rue de Sèvres, 75015 Paris, France
E-mail: guillaume.canaud@inserm.fr
Phone : +33144381773

Abstract

Proliferative glomerulonephritis is a severe condition often leading to kidney failure. There is a significant lack of effective treatment for these disorders. Here, following the identification of a somatic *PIK3CA* gain-of-function mutation in podocytes of a patient, we demonstrate using multiple genetically engineered mouse models, single-cell RNA sequencing and spatial transcriptomics the crucial role played by this pathway for proliferative glomerulonephritis development by promoting podocyte proliferation, dedifferentiation and inflammation. Additionally, we show that alpelisib, a PI3Kα inhibitor, improves glomerular lesions and kidney function in different mouse models of proliferative glomerulonephritis and lupus nephritis by targeting podocytes. Surprisingly, we determined that pharmacological inhibition of PI3Kα affects B and T lymphocyte population in lupus nephritis mouse models with decrease in the production of proinflammatory cytokines, autoantibodies and glomerular complement deposition, which are all characteristic features of PI3K delta (PI3Kδ) inhibition, the primary PI3K isoform expressed in lymphocytes. Importantly, PI3Kα inhibition does not impact lymphocyte function under normal conditions. These findings were then confirmed in human lymphocytes isolated from patients with active lupus nephritis. In conclusion, we demonstrate the major role played by PI3Kα in proliferative glomerulonephritis and show that in this condition, alpelisib acts on both podocytes and the immune system.

Introduction

PI3Kα is a lipid kinase that is widely expressed in various tissues and plays a crucial role in controlling signaling pathways involved in cell proliferation, motility, survival, and metabolism(1). The *PIK3CA* gene codes for the alpha subunit of PI3K (p110α), which has a molecular weight of 110 kDa. Following its activation through tyrosine kinase receptors, p110α converts phosphatidylinositol 4,5-bisphosphate (PtdIns(4,5)P2) to phosphatidylinositol 3,4,5-trisphosphate (PtdIns(3,4,5)P3 or PIP3) at the plasma membrane. This conversion leads to the recruitment of PDK1, which phosphorylates AKT on Thr^{308} residue and initiates downstream cellular effects(1). Additionally, PI3Kα regulates various other pathways including the Rho/Rac1 signaling cascade(2).

Somatic gain-of-function mutations in the *PIK3CA* gene have been described in patients and associated with overgrowth syndromes and are called *PIK3CA*-Related Overgrowth Syndrome (PROS)(3),(4). Individuals with PROS typically exhibit complex tissue malformations such as abnormal vessels, disorganized adipose tissue, muscle hypertrophy and bone deformations(5-10). In previous research, we identified alpelisib, a PI3Kα inhibitor, as a promising treatment option and demonstrated its effectiveness in both mouse models and PROS patients(11). These findings were further validated in the EPIK P1 clinical trial (NCT04285723)(12), which led to the recent accelerated approval of alpelisib by the US FDA for PROS patients above two years of age.

In our initial report, the first PROS patient (referred to as patient 1) had kidney dysfunction with nephrotic range proteinuria before beginning alpelisib treatment(11). The patient was carrying a somatic *PIK3CA* p.H1047R variant that had been previously identified in a skin biopsy (c.3140 A>G, COSMIC Genomic mutation ID: 55873195)(11). The kidney disease of patient 1 occurred in a complex medical context involving severe vascular malformations (including a combination of vein and lymphatic anomalies as well as arteriovenous shunts), paraplegia with vesicoureteral reflux, severe congestive heart failure, and the use of rapamycin (an mTOR inhibitor)(13). While administering alpelisib to address the patient's overall condition, we noticed an improvement in both kidney function and proteinuria(11). This prompted us to

investigate the role of PI3Kα in the patient's kidney disease and ultimately identify this kinase as a promising target for addressing proliferative glomerulonephritis.

Results

A patient with PIK3CA gain-of-function mutation in podocytes

Patient 1 underwent a kidney biopsy prior to initiating alpelisib treatment, which revealed a complex glomerulonephritis characterized by focal and segmental glomerulosclerosis (FSGS), with podocyte hyperplasia and hypertrophy, collapsing aspect and pseudo-crescentic formation (**Fig. 1A and Supplemental Fig. 1A**). Notably, there were no immune deposits observed. The biopsy also indicated extensive fibrosis (>80% of the parenchyma) accompanied by tubular dilation, casts, and infiltration of inflammatory cells (**Fig. 1A and Supplemental Fig. 1A**). Immunofluorescence studies showed activation of the AKT/mTOR pathway in podocytes (**Fig. 1B and Supplemental Fig. 1B**). Initially, we speculated that these lesions were a consequence of the patient's complicated medical condition involving vesicoureteral reflux, congestive heart failure, and rapamycin usage. After discontinuing rapamycin, no improvement was observed regarding proteinuria or kidney function(11). As previously reported, because of the severity of the PROS condition, we were granted the authorization to administer alpelisib, which is an approved isoform selective PI3Kα inhibitor(11). Treatment with this medication resulted in the reduction of different malformations and a complete recovery from congestive heart failure(11). Intriguingly, we observed improvement in the high amount of proteinuria and the stabilization of kidney function(11). This indicated that the patient may carry a *PI3KCA* mutation in the kidney epithelial cells. To investigate this possibility, we first performed in situ PCR using fluorescently labeled mismatched primers designed to specifically amplify mutant that was previously identified in a skin biopsy using Next Generation Sequencing(11) (p.H1047R, c.3140 A>G, COSMIC Genomic mutation ID: 55873195) and wild-type *PIK3CA* alleles on a paraffin-embedded kidney biopsy section(14). T-47D cells were employed as positive controls (**Supplemental Fig. 1C**). We observed the presence of the *PIK3CA* mutant alleles in various types of glomerular cells including cells evocative of podocytes (**Fig. 1C**). Unfortunately, due to technical limitations, we were unable to perform coimmunostaining to specifically identify the affected cell types. To confirm the presence of the mutation, we performed droplet digital PCR (ddPCR) of glomeruli

isolated from the kidney biopsy from patient 1 using laser capture microdissection (**Supplemental Fig. 1D**). While control biopsies obtained from diabetic patients did not reveal any alteration in *PIK3C*A alleles, ddPCR of the glomeruli from patient 1 demonstrated the presence of the *PIK3CA H1047R* mutation at a mosaic fraction of 8% (**Supplemental Fig. 1E**). We concluded that patient 1 was carrying the *PIK3CA* gain-of-function mutation in glomerular epithelial cells.

PIK3CA gain-of-function mutation in podocytes causes progressive proliferative glomerulonephritis in mice

Considering the glomerular profile of kidney dysfunction in patient 1, the presence of the *PIK3CA* variant in glomerular cells and the substantial decrease in proteinuria upon the introduction of alpelisib, we decided to create a mouse model of the *PIK3CA* gain-of-function mutation within podocytes. We took advantage of the transgenic mouse strain, *R26StopFLP110**, which after breading with *Cre* recombinase mice, expresses a dominant active *PI3KCA* transgene(11). *R26StopFLP110** mice were crossed with *Podocin Cre* mice to generate $PIK3CA^{Pod}$ animals that expressed the over-activated form of PIK3CA. To follow *Cre* recombination, $PIK3CA^{Pod}$ mice were interbred with $Gt(ROSA)26Sor^{tm4(ACTB-tdTomato,-EGFP)Luo/J}$ mice to create $PIK3CA^{Pod-HET}$ mice(15). These mice express a cell membrane localized tdTomato fluorescent protein in all tissues that is replaced by GFP after *Cre* recombination. At birth, $PIK3CA^{Pod-HET}$ mice were indistinguishable from *WT* control littermates (referred to hereafter as $PIK3CA^{WT}$). However, $PIK3CA^{Pod-HET}$ mice progressively developed albuminuria after 3 months of age with slowly declining kidney function (**Fig. 1D, 1E and Supplemental Fig. 1F**) and reduced survival (**Fig. 1F**). Compared to the controls, starting at the age of 3 months, $PIK3CA^{Pod-HET}$ mice demonstrated glomerular lesion mixing pseudo-crescentic formation with cellular proliferation such as that observed in patient 1 (**Fig. 1A, 1G and Supplemental Fig. 1G**). Optical microscopy revealed hypertrophic podocytes with intracytoplasmic vacuoles as well as protein casts and infiltration of inflammatory cells (**Fig. 1G, Supplemental Fig. 1G and 1H**). Costaining between Nephrin and CD44 revealed

progressive and extensive formation of crescentic lesions in glomeruli from *PIK3CA*$^{Pod\text{-}HET}$ mice compared to controls (**Supplemental Fig. 1I**). Crescents were visible starting from the age of 5 months and worsening with age (**Supplemental Fig. 1I and 1J**). Transmission electron microscopy showed swollen hypertrophic podocytes with microvillous transformation, lipid vacuolization and focal foot process effacement (**Supplemental Fig. 2A**). The glomerular basement membrane demonstrated thickening and wrinkling, typical features of FSGS lesion and more specifically collapsing glomerulopathy (**Supplemental Fig. 2A**). Immunofluorescence experiments confirmed the activation of the AKT/mTOR pathway specifically in podocytes of *PIK3CA*$^{Pod\text{-}HET}$ mice (**Fig. 1H, 1I and Supplemental Fig. 2B**). One of the main characteristics of podocyte injury is the loss of differentiation markers. We decided to study cellular differentiation by analyzing the expression of WT1, which is a transcription factor that marks mature podocytes, nephrin, podocin and nestin, proteins that contribute to foot process formation in differentiated podocytes. Staining experiments revealed a significant loss of podocyte differentiation markers in *PIK3CA*$^{Pod\text{-}HET}$ mice compared to controls (**Fig. 1J, 1K and Supplemental Fig. 2C-2E**). Mechanistically, PI3Kα plays a role in cell growth and proliferation. Therefore, we examined for proliferation within the glomeruli of these mouse models using Ki-67, which is a marker for cellular proliferation. While the number of Ki-67^{+} cells was very low in control mice, a notable increase in the number of Ki-67+ cells was observed within the glomeruli of *PIK3CA*$^{Pod\text{-}HET}$ mice. Immunofluorescence experiments using Ki-67, GFP and PDGFRβ revealed that both, podocytes but also mesangial cells were undergoing proliferation (**Fig. 1L, 1M and Supplemental Fig. 2F-2H**). We further observed that proliferation started at 3 months of age and was increasing with aging (**Supplemental Fig. 2I and 2J**). These findings align with the notion that cells undergoing cell cycle entry tend to lose their differentiation markers(16). Then, using an Amnis ImageStream® system, we confirmed that podocytes isolated from *PIK3CA*$^{Pod\text{-}HET}$ mice were hypertrophic compared to controls (**Fig. 1N**). Flow cytometry experiments further demonstrated a correlation between podocyte size and the level of activation of the AKT/mTOR pathway, particularly the mTORC1 pathway (**Supplemental Fig. 2K**). Indeed, we concluded that the excessive activation of PI3Kα in

podocytes leads to both dedifferentiation and proliferation, which results in FSGS with progressive proteinuria and kidney dysfunction. This mouse model effectively recapitulates the kidney phenotype observed in patient 1.

To investigate the impact of allele dosage on the overactivation of the PI3Kα pathway, we generated mice that were homozygous for the *PIK3CA* mutation specifically in podocytes and referred to them as *PIK3CA*$^{Pod\text{-}HO}$ mice. At birth, *PIK3CA*$^{Pod\text{-}HO}$ mice were initially indistinguishable from controls. However, these mice rapidly developed a significant amount of albuminuria (**Fig. 1O**) with reduced survival rates (**Fig. 1F**). Histological analysis conducted at the age of 12 weeks revealed severe proliferative glomerulonephritis (**Supplemental Fig. 3A and 3B**). Transmission electron microscopy revealed hypertrophic podocytes, lipid vacuolization, extensive focal foot process effacement and widespread glomerular basement membrane thickening (**Supplemental Fig. 3C**). Consistently, we observed dedifferentiation, recruitment of the AKT/mTOR pathway, immune cell infiltration and increased proliferation in both, podocytes and mesangial cells (**Supplemental Fig. 3D-3L)**. These findings demonstrate that the cumulative activation of the PI3Kα pathway is associated with a more severe disease phenotype.

Overactivation of PI3Kα pathway in podocytes is associated with changes in cell fate determination

Podocytes are postmitotic cells with limited possibilities of proliferation and renewal. However, under certain pathological circumstances, podocytes can reenter into the cell cycle and become dedifferentiated(17). To identify the early transcriptional changes in podocytes associated with podocyte *PI3KCA* gain-of-function mutation, we performed single-cell RNA sequencing (scRNA-seq) and mapped kidney cells from *PIK3CA*^{WT} and *PIK3CA*$^{Pod\text{-}HET}$ mice (**Supplemental Fig. 4A**). To increase the podocyte population, which counts as only 0.18% of the normal mouse kidney(18), we enriched the glomeruli with an injection of magnetic beads. Two mice for each condition were pooled to increase the number of cells. A total of 49,600

cells were isolated and sequenced. After data normalization and filtering (**Supplemental Fig. 4B**), 26,508 cells were further analyzed. The unsupervised clustering of the entire pooled dataset identified 20 clusters (**Fig. 2A and Supplemental Fig. 4C**). With well-established cell-type markers from the literature, we annotated broad cluster classes (**Fig. 2A**, **2B**, **Supplemental Fig. 4D** and **Supplemental Table 1**). We annotated 6 podocyte clusters based on the expression of *Nphs2*, *Synpo*, *Podxl*, *Pdpn*, and *EGFP* (**Fig. 2B and Supplemental Fig. 4D**). We decided to include some of the clusters with weaker expressions of podocyte markers (Podocyte-4, -5, and -6) with the aim of understanding different cell states of podocytes. The monocle single-cell trajectory from 6 podocyte clusters resulted in 5 distinct states (**Fig. 2C and Supplemental Fig. 4E**). While podocyte-2, 4, and 5 clusters showed similar pseudo-temporal ordering distributions, podocyte-1 and 3 clusters were distinct (**Fig. 2C**). The podocyte-1 cluster was activated for the PI3K-AKT pathway and signaling pathways regulating pluripotency; the podocyte-3 cluster was enriched for inflammatory pathways (**Supplemental Table 2**). In *PIK3CA*^{WT} mice, podocyte clusters accounted for approximately 10% of the whole analyzed cells, while in *PIK3CA*$^{Pod\text{-}HET}$ mice, it increased to 23.7%, which supported the proliferation of podocytes (**Fig. 3A and 3B**). We finally observed that podocytes of *PIK3CA*$^{Pod\text{-}HET}$ mice showed a significant differential expression of genes that are known to be upregulated in FSGS(19), such as *Wnt4*, *metallothioneins Mt1* and *Mt2*, *Col1a2*, *Col4a3*, *Col4a4*, or *Il18*, which are related to the inhibition of apoptosis, dedifferentiation, and proliferation (**Supplemental Fig. 4F**). These results indicate that PI3K-AKT pathway activation in podocytes drives podocyte fate transition.

Alpelisib improves PIK3CA^{Pod} *mouse models*

Patient 1 demonstrated renal failure amelioration upon the introduction of alpelisib(11). However, the concurrent shrinkage of vascular malformations and correction of severe congestive heart failure caused by alpelisib treatment added potential confounding factors(11). To gain a better understanding of whether alpelisib was effective in improving kidney dysfunction in our patient, we first investigated the ability of the drug to diffuse into the kidneys.

Liquid chromatography-mass spectrometry (LC-MS) analysis of mouse kidneys revealed that alpelisib was detectable 1.5 hours after oral administration with concentrations similar to those found in skeletal muscle and the liver (**Supplemental Fig. 5A**). Subsequently, we administered alpelisib orally over a period of 3 weeks to 3-month-old *PIK3CA*$^{Pod\text{-}HET}$ mice (**Supplemental Fig. 5B**). Treatment with alpelisib resulted in a gradual reduction in albuminuria (**Supplemental Fig. 5C**) along with inhibition of the AKT/mTOR pathway in glomeruli (**Supplemental Fig. 5D and 5E**), increased expression of Nephrin and Synaptopodin (**Supplemental Fig. 5F and 5G**) and a decrease in podocyte size (**Supplemental Fig. 5H**). scRNA-seq analysis of kidney cells from alpelisib-treated *PIK3CA*$^{Pod\text{-}HET}$ mice revealed that podocyte populations were restored to 11.7% compared to vehicle-treated *PIK3CA*$^{Pod\text{-}HET}$ mice (**Fig. 3A and 3B**). In addition, we observed that alpelisib treatment was associated with the correction of various gene expression anomalies **(Supplemental Fig. 4F and 4G**). These results indicate that alpelisib was able to successfully interfere with podocyte fate transition induced by overactivation of the PI3K-AKT pathway.

Then, we administered either the vehicle or alpelisib to the most severe model, *PIK3CA*$^{Pod\text{-}HO}$ mice, at 10 weeks of age when proteinuria had already been established (**Supplemental Fig. 6A and 6B**). The treatment period lasted for two consecutive weeks. Throughout the treatment period, we observed a progressive reduction in albuminuria in the alpelisib-treated mice, which was accompanied by a significant improvement in kidney function (**Supplemental Fig. 6C-6E**). At the end of the treatment period, the mice were sacrificed and histological analysis of the kidneys revealed that *PIK3CA*$^{Pod\text{-}HO}$ mice treated with alpelisib exhibited preserved glomeruli compared to the vehicle-treated group (**Supplemental Fig. 6F and 6G**). Podocyte differentiation markers were still expressed at protein levels in the alpelisib-treated group compared to vehicle-treated mice (**Supplemental Fig. 6H**). The activation of the AKT/mTOR pathway was attenuated following alpelisib treatment (**Supplemental Fig. 6H-6J**). Mechanistically, the alpelisib treatment was associated with a decrease in glomerular cell proliferation (**Supplemental Fig. 6K and 6L**).

To better assess the improvement and potential reversibility of kidney lesions, we conducted unilateral nephrectomy in both *PIK3CA*$^{Pod\text{-}HO}$ mice and controls at 8 weeks of age (**Fig. 4A**). The mice were randomly assigned to receive either the vehicle or alpelisib treatment from postoperative day 1 for a duration of 2 weeks (**Supplemental Fig. 7A and 7B**). We first observed that uninephrectomized *PIK3CA*^{WT} mice, whether treated with the vehicle or alpelisib, did not display any notable phenotype with no presence of proteinuria or kidney dysfunction (**Fig. 4B-4K and Supplemental Figure 7C**). In contrast, *PIK3CA*$^{Pod\text{-}HO}$ mice treated with the vehicle following surgery rapidly developed a significant amount of proteinuria, kidney dysfunction, severe glomerular lesions, increased AKT activity, and decreased expression of podocyte markers (**Fig. 4B-4K and Supplemental Figure 7C**). However, *PIK3CA*$^{Pod\text{-}HO}$ mice treated with alpelisib following surgery demonstrated a significantly reduced amount of proteinuria, no kidney dysfunction, preserved glomerular lesions, a higher expression of podocyte markers and decreased activation of podocytes AKT/mTOR pathway (**Fig. 4B-4K and Supplemental Figure 7C**). Interestingly, the trajectory of albuminuria had an opposite effect following uninephrectomy in *PIK3CA*$^{Pod\text{-}HO}$ mice treated with alpelisib compared to those treated with the vehicle (**Fig. 4L**). Furthermore, a comparison of glomerular lesions before and after surgery indicated that alpelisib treatment was associated with a potential reversal of kidney lesions in *PIK3CA*$^{Pod\text{-}HO}$ mice (**Fig. 4M**). Based on these findings, we concluded that alpelisib was able to prevent and potentially reverse the disease in a mouse model carrying *PIK3CA* gain-of-function mutation in podocytes.

Alpelisib improves different mouse models of proliferative glomerulonephritis

PIK3CA^{Pod} mouse models developed characteristics resembling collapsing glomerulopathy and extracapillary disorders. In humans, collapsing glomerulopathy can occur as a primary condition or as a secondary manifestation of other diseases such as HIV or toxic exposures(20). On the other hand, crescentic glomerulonephritis is the hallmark of severe autoimmune diseases affecting the kidneys such as lupus nephritis and antineutrophil cytoplasmic antibody (ANCA) vasculitis. Both types of glomerular lesions are associated with

significant kidney damage and poor renal survival. To further investigate if targeting the AKT/mTOR pathway with these disorders are reasonable, we first conducted immunofluorescence experiments in human patient kidneys. These experiments confirmed the activation of the AKT/mTOR pathway in podocytes, compared to kidney biopsies from healthy individuals who underwent a biopsy because of a low-rate proteinuria (<1 g/L) or mild hematuria with normal histological examination and no immunofluorescent deposits (**Fig. 5A, 5B, Supplemental Fig. 8A and 8B)**.

We further investigated the glomerular spatial transcriptomic changes in patients with extracapillary disorders using the GeoMx^{TM} digital spatial profiler technology. Kidney biopsies from four patients with highly active lupus nephritis (LN) and the four healthy controls were selected for analysis (**Supplemental Fig. 8B and 8C**). A total of 49 glomeruli were selected as regions of interest (ROIs) (33 ROIs for LN and 16 ROIs for controls). More than 18,000 genes were assayed in these ROIs (**Supplemental Fig. 8D**). The glomerular transcriptomes of LN samples showed distinct and broader clustering patterns compared to those of control samples (**Supplemental Fig. 8E**). Consistent with single-cell RNA sequencing analysis in *PIK3CA*$^{Pod\text{-}HET}$ mice, the gene expression profiles in LN glomeruli indicated a dedifferentiated state and elevated levels of inflammation-related transcripts (**Fig. 5C and 5D**). We separately stained pAKT^{Ser473} in LN samples and classified each ROI based on the level of pAKT^{Ser473} activity with 20 ROIs classified as activity-high and 13 ROIs classified as activity-low (**Supplemental Fig. 8F**). The higher pAKT^{Ser473} activity correlated with gene set enrichment of the WNT pathway and significant upregulation of *Wnt4* (**Fig. 5E and 5F**). Indeed, *PIK3CA*$^{Pod\text{-}HET}$ mutant mice demonstrate similar transcriptomic changes that closely resemble patterns observed in LN patients.

Based on these findings and the previous reports on the association between podocyte and their disease pathology(21-24), we investigated whether the inhibition of PIK3CA could be a potential therapeutic approach for collapsing glomerulopathy and extracapillary glomerular nephritis.

We initially examined *Tg26*^{He} mice, which serve as a model for collapsing glomerulopathy(25). Typically, these transgenic mice develop proteinuria around 24 days of age, exhibit severe kidney lesions, and die between 2 and 9 months of age(25). We observed activation of the AKT/mTOR pathway in podocytes of 4-week-old *Tg26*^{He} mice compared to controls (**Supplemental Fig. 9A and 9B**). Since *Tg26*^{He} mice is very variable for its severity and course of the disease (**Supplemental Fig. 9C)**, we decided to employ the experiment model of unilateral nephrectomy, to standardize the variability and to accelerate the disease progression. This approach would in addition expedite the development of kidney lesions and allow a direct comparison of paired kidneys before and after surgery. At four weeks old, both *Tg26*^{He} and *Tg26*^{WT} mice underwent uninephrectomy followed by a random assignment to receive either the vehicle (*Tg26*^{WT} n=16, *Tg26*^{He} n=15) or alpelisib (*Tg26*^{WT} n=18, *Tg26*^{He} n=19) treatment for a duration of four weeks (**Fig. 6A**). Upon sacrifice, we observed that while the surfaces of the kidneys in uninephrectomized *Tg26*^{WT} or *Tg26*^{He} treated with alpelisib appeared regular and smooth, the surfaces of the kidneys from *Tg26*^{He} mice treated with the vehicle exhibited irregularities (**Supplemental Fig. 9D**). Kidney function, as well as albuminuria, were significantly improved in *Tg26*^{He} mice treated with alpelisib compared to those treated with the vehicle (**Fig. 6B-6D**). Additionally, the ratio of kidney-to-body weight showed that kidney hypertrophy caused by uninephrectomy was improved in uninephrectomized *Tg26*^{He} mice treated with alpelisib (**Supplemental Fig. 9E**). Histological examination of the kidneys revealed that alpelisib-treated uninephrectomized *Tg26*^{He} mice exhibited fewer glomerular lesions (**Fig. 6E and 6F**) and maintained the expression of podocyte markers (**Fig. 6G and Supplemental Fig. 9F**). Furthermore, the expression of *Col1a*, *Col3a* and *Lcn2* was reduced in the alpelisib-treated group (**Supplemental Fig. 9G-9I**). Mechanistically, the AKT/mTOR pathway in glomeruli showed significant suppression in mice treated with alpelisib (**Fig. 6H-6I, and Supplemental Figure 9J-9K**). Finally, we compared the kidney function, albuminuria and glomerular lesion score before and after nephrectomy and observed that the rate of disease

progression in mice treated with alpelisib was lower compared to those treated with the vehicle (**Fig. 6J-6M**).

To specifically investigate the role of PI3Kα in podocytes during collapsing glomerulopathy, we employed a genetic approach to remove *PIK3CA* specifically in these cells. To achieve this, we generated *PIK3CA*$^{Podo\text{-}KO}$ mice by crossing *Podocin Cre* mice with *PIK3CA*$^{lox/lox}$ mice. These mice were subsequently backcrossed with the *FVB/N* strain for 10 generations and bred with *Tg26* mice to obtain *Tg26*^{He}*PIK3CA*$^{Podo\text{-}KO}$. These mice were viable and had no particular phenotype at birth. However, as they aged, we observed that *Tg26*^{He}*PIK3CA*$^{Podo\text{-}KO}$ mice displayed reduced levels of albuminuria, milder glomerular lesions, decreased kidney fibrosis, and improved kidney function compared to control littermate *Tg26*^{He}*PIK3CA*$^{Podo\text{-}WT}$ mice (**Fig. 7A-7L**). Importantly, the deletion of *PIK3CA* in podocytes alone was sufficient to alleviate the severity of collapsing glomerular lesions and improve the kidney function in the *Tg26*^{He} mouse model. Next, we attempted to determine whether removing *PIK3CA* in podocytes later in life, when glomerular lesions were already established, could lead to an improvement in kidney lesions. For this purpose, we generated *PIK3CA*$^{iPodo\text{-}KO}$ mice by backcrossing tamoxifen-inducible *Podocin Cre* mice with *PIK3CA*$^{lox/lox}$ mice on the *FVB/N* strain (10 generations) and crossing them with *Tg26*^{He} mice to obtain *Tg26*^{He}*PIK3CA*$^{iPodo\text{-}KO}$. Cre recombination was induced in 3-week-old *Tg26*^{He}*PIK3CA*$^{iPodo\text{-}KO}$ mice, and the mice were sacrificed at 12 weeks. We observed that these mice exhibited improved glomerular lesion scores and reduced albuminuria compared to the control group (**Fig. 8A and 8B**). Similarly, when Cre recombination was induced at 6 weeks of age, kidney lesions were reversed by 12 weeks (**Fig. 8A and 8C**). However, when Cre recombination was induced at a later time point, specifically at 8 weeks of age, the progression of the disease was no longer affected, which indicated that reversing the phenotype becomes challenging once the kidney lesions have become too severe (**Fig. 8A and 8D**). In this model of collapsing glomerulopathy, we determined that the activation of PI3Kα in podocytes is significantly important and inhibition holds great promise as a potential therapeutic approach.

Next, we investigated the impact of PI3Kα inhibition in extracapillary glomerulonephritis, particularly in lupus mouse models. Our initial approach involved using *NZBWF1/J* mice, a well-established model that exhibits lupus-like nephritis(26). *NZBWF1/J* mice gradually develop immune glomerulonephritis characterized by proteinuria and kidney dysfunction starting around 25 weeks of age(26). However, this model is also known for its variability(26). For the same reason for *Tg26*^{He} mice model, we employed the uninephrectomy model and performed uninephrectomy on 30 female mice at 24 weeks of age (**Supplemental Fig. 10A**). Notably, the incidence and severity of symptoms are more pronounced in females and we used only females for our study. The mice were then randomly assigned to receive either the vehicle (n=15) or alpelisib treatment (n=15) for a duration of 4 weeks. At the end of the treatment period, the mice were sacrificed and their kidney histology was compared to samples obtained during the uninephrectomy procedure. At the time of uninephrectomy, no discernible differences were observed between the two groups in terms of phenotypic characteristics including proteinuria and the kidney-to-body weight ratio (**Supplemental Fig. 10B and 10C**). However, upon sacrifice, mice treated with alpelisib exhibited significant reductions in albuminuria (**Fig. 9A**) and blood urea nitrogen levels (**Fig. 9B**). Furthermore, the kidney-to-body weight ratio was notably decreased in uninephrectomized *NZBWF1/J* mice receiving alpelisib (**Fig. 9C**). From a histological standpoint, the alpelisib-treated mice displayed preserved glomeruli compared to those receiving the vehicle (**Fig. 9D and 9E**). While glomerular lesions worsened considerably in the vehicle-treated uninephrectomized *NZBWF1/J* mice, they remained stable in the alpelisib group (**Fig. 9E**). Additionally, the alpelisib treatment resulted in the attenuation of AKT/mTOR pathway activation within the glomeruli (**Fig. 9F and 9G**). The expression of *Col1a* and *Col3a* mRNA as well as *Tnfα* was significantly reduced in mice treated with alpelisib (**Fig. 9H, 9I, and 9J**). Moreover, the group of uninephrectomized *NZBWF1/J* mice treated with alpelisib demonstrated marked improvements in podocyte differentiation markers (**Fig. 9F, 9K and Supplemental Fig. 10D**). In *NZBWF1/J* mice treated with alpelisib, we observed a partial correction of anemia and a significant increase in platelet count (**Supplemental Fig. 10E**). Then, we explored glomerular

IgG, IgM and C3 deposits and unexpectedly observed a significant reduction of deposits in glomeruli mice receiving alpelisib (**Fig. 9L-9N, Supplemental Fig. 10F**). To obtain further insight, we measured the level of circulating dsDNA, which is a marker of systemic lupus erythematosus (SLE) disease activity, and noticed a significant decrease in *NZBWF1/J* mice treated with alpelisib (**Supplemental Fig. 10G**). Notably, the spleen size was significantly reduced in both sham and uninephrectomized mice treated with alpelisib (**Supplemental Fig. 10H**). A blood test revealed that alpelisib treatment was associated with a reduction in white blood cell count, particularly on lymphocytes and monocytes (**Supplemental Fig. 10E**). Flow cytometry of peripheral blood mononuclear cells (PBMCs) did not indicate any significant changes in the distribution of the lymphocyte population (**Supplemental Fig. 10I**). An examination of the spleen revealed a decrease in both the B and T cell population in *NZBWF1/J* mice treated with alpelisib (**Supplemental Fig. 10I**). The B cell population was also significantly impacted in lymph nodes and bone marrow (**Supplemental Fig. 10I**). These findings were unexpected since PI3Kδ is the predominantly expressed isoform in leukocytes(27-30), and it was not anticipated that alpelisib would have an impact on the lymphocyte population. To understand if alpelisib was able to modify the lymphocyte population in wild-type mice, we conducted a study where we administered either the vehicle or alpelisib daily to 8-week-old *FVB/NJ* wild type mice for 4 consecutive weeks. Afterwards, we examined the lymphocyte population and found no changes in white blood cell count (**Supplemental Fig. 11A**) or in lymphocyte population in lymph nodes, spleen, or PBMCs of alpelisib-treated mice compared to vehicle treated mice (**Supplemental Fig. 11B**). These results indicate that alpelisib specifically targeted lymphocytes in *NZBWF1/J* mice. Next, we measured the serum levels of circulating proinflammatory cytokines in *NZBWF1/J* mice treated with either the vehicle or alpelisib and observed a reduction in cytokines in alpelisib-treated mice (**Supplemental Fig. 10J**). Collectively, these findings indicate that alpelisib might exert its effects on both podocytes and lymphocytes in *NZBWF1/J* mice, which results in the attenuation of lupus nephritis.

To validate the significance of these findings, we conducted a further investigation on the effects of alpelisib in *MRL/MpJ-Fas^{lpr}/J* mice (referred here as *MRL-lpr*), which is another model of lupus nephritis(31). These mice possess homozygous Fas mutations and typically develop an autoimmune disease resembling systemic lupus, which is characterized by lymphadenoproliferation, progressive renal failure, and skin lesions(32). Female *MRL-lpr* mice usually succumb to the disease by 18-20 weeks old. To begin, we randomly assigned 8-week-old female *MRL-lpr* mice prior to the complete onset of the disease to receive either the vehicle or alpelisib. The administration of alpelisib resulted in a modest but significant increase in life expectancy (**Fig. 10A**). It is important to note that mice were dying from well characterized skin lesions and voluminous compressive lymph nodes around the neck(33). Furthermore, *MRL-lpr* mice treated with alpelisib exhibited reduced proteinuria compared to those treated with the vehicle (**Fig. 10B**). More strikingly, the comparison of albuminuria before and after treatment introduction showed opposite trajectories. Specifically, *MRL-lpr* mice treated with alpelisib demonstrated an improvement in proteinuria, which suggests potential reversibility of the disease (**Fig. 10C and 10D**). At sacrifice, *MRL-lpr* mice treated with alpelisib showed a tendency toward a lower kidney-to-body weight ratio and a significant decrease in spleen weight compared to the vehicle-treated mice (**Fig. 10E and 10F**). An examination of the kidneys revealed that alpelisib treatment was associated with fewer glomerular lesions compared to the vehicle-treated mice (**Fig. 10G and 10H**) and improved kidney function (**Fig. 10I and 10J**). To further demonstrate the potential reversibility of the glomerular lesion with alpelisib, we randomly assigned either the vehicle or alpelisib to 12-week-old *MRL-lpr* male and female mice. At this age, kidney lesions are already established. Mice were then treated for 4 consecutive weeks (**Supplemental Fig. 12A**). Alpelisib was again associated with proteinuria reduction (**Supplemental Fig. 12B**). At the histological level, we found that the glomerular lesion score was improved in the alpelisib group as well as *Cola1* and *Cola3* mRNA expression (**Fig. 10K-10N**). Consistently, the glomerular AKT/mTOR pathway was inhibited in the group of alpelisib-treated mice (**Fig. 10O-10S**). The expression of podocyte differentiation markers was increased in alpelisib mice compared to the vehicle (**Fig. 10O, 10S and**

Supplemental Fig. 12C). Therefore, we explored circulating dsDNA antibodies. At the initiation of the treatment, there were no significant differences between the two groups (**Supplemental Fig. 12D**). However, as the treatment progressed, the alpelisib-treated group exhibited a significant reduction in circulating dsDNA antibodies (**Fig. 10T**). Additionally, we observed a remarkable decrease in spleen in the alpelisib-treated group of mice (**Supplemental Fig. 12E**). Consistent with the results obtained in the previous mouse model, blood tests revealed that anemia and platelet count were corrected in *MRL-lpr* mice treated with alpelisib compared to the control group (**Supplemental Fig. 12F**). Furthermore, alpelisib-treated mice demonstrated a decrease in white blood cell count, which was primarily due to reductions in lymphocytes and monocytes (**Supplemental Fig. 12F**). Flow cytometry analysis revealed a significant reduction in B cells both in its absolute number and percentage within the spleen of alpelisib-treated *MRL-lpr* mice and a decrease in B cell percentage in PBMCs, bone marrow and lymph nodes (**Supplemental Fig. 12G**). These changes were associated with reduced serum levels of circulating proinflammatory cytokines in the alpelisib-treated group of mice (**Supplemental Fig. 12H**). Finally, IgG, IgM and C3 deposits were significantly reduced in glomeruli from *MRL-lpr* mice receiving alpelisib (**Supplemental Fig. 12I and 12J**). We concluded that alpelisib exerts its effects on both podocytes and the immune compartment in *MRL-lpr* and *NZBWF1/J* mice.

Next, we attempted to determine the relevance of these observations in patients with lupus nephritis. We obtained PBMCs from 4 patients with active class 4 lupus nephritis (LN). The treatment regimens for each patient are detailed in **Supplemental Fig. 13A**. CD19 positive B cells and CD3 positive T cells were isolated from PBMCs and cultured in vitro (**Supplemental Fig. 13B-13E**). These cells were then stimulated and exposed to either the vehicle or varying doses of alpelisib. Stimulation induced a significant level of S6RP phosphorylation in both CD19 and CD3 cells (**Fig. 11A, 11B and Supplemental Fig. 13E**), and it also led to the expression of CD69, an activation marker, in CD3 positive cells (**Fig. 11B**). Importantly, this response was observed in all patients except for CD19 cells derived from patient LN 1, who received obinutuzumab, which is a humanized anti-CD20 monoclonal antibody, a few weeks

prior (**Fig. 11A and Supplemental Fig. 13A**). Crucially, the treatment with alpelisib effectively suppressed S6RP phosphorylation in both types of cells and reduced CD69 expression in T cells (**Fig. 11A and 11B**). Finally, we observed that the levels of inflammatory cytokines in the supernatant of cultured CD3 cells were decreased with the alpelisib treatment (**Fig. 11C and Supplemental Figure 14A**). These findings suggest that alpelisib treatment affects both activated B and T cells in lupus patients, which leads to a decrease in their inflammatory markers. These results support the findings observed in mouse models of lupus nephritis.

Discussion and conclusion

In this work, starting from the 1st description ever of a patient carrying a somatic gain-of-function mutation of *PIK3CA* in glomerular epithelial cells, we demonstrated the crucial role of this pathway is podocyte proliferation, hypertrophy and crescentic formation. Single-cell RNA sequencing revealed that PI3Kα overactivation triggered developmental programs in podocytes and resulted in dedifferentiation and inflammation. Using genetic tools and pharmacological PI3Kα inhibitor, we present compelling evidence supporting the targeting of this pathway as a potential treatment approach for proliferative glomerulonephritis. Furthermore, we show for the first time that B and T cells from lupus mouse models and from patients with lupus nephritis activate the PI3Kα pathway, and treatment with alpelisib reduces the synthesis of proinflammatory cytokines.

The PI3Kα pathway is widely recognized for its ability to regulate cell growth, cell proliferation, and stemness in different cellular settings(34, 35). Notably, the activation of PI3Kα contributes to the maintenance of stemness and influences the destiny of stem cells, particularly through its interaction with the WNT pathway(36-38). Our research findings align with previous studies demonstrating that activation of the WNT pathway in podocytes may promote proliferation, dedifferentiation, and the formation of collapsing glomerulopathy lesions(39). Interestingly, we also observed a certain level of reversibility in glomerular lesions, which has been previously suggested(39, 40), and which is important when we think of the drug application for chronic kidney disease in clinics. These studies highlighted the role of mTORC1 in podocytes in physiological and disease states, while this work is the first devoted to PI3Kα(41).

Targeting podocytes as a therapeutic for kidney disease therapy has been of great interest over the decades but yet, unachieved(42). Rapamycin, a mTOR pathway inhibitor, has been investigated in treating various kidney diseases, but it has been mainly restricted to kidney transplantation(43-45) and tuberous sclerosis disorders(46) due to its potential nephrotoxicity(13). By acting at a higher level on the pathway, alpelisib which is a cytostatic drug with an acceptable safety profile in patients with PROS and without described

nephrotoxicity, holds promises to treat various proliferative glomerular diseases by directly targeting podocytes.

This study further presents the first evidence of the impact of pharmacological inhibition of PI3Kα on lymphocytes derived from lupus models and patients. In the field of leukocyte biology, the role of PI3Kα is not prominent and its inhibition in lupus, particularly compared to the delta isoform of PI3K(27-30), has not been explored until now. Surprisingly, our findings indicate that the use of alpelisib, which is not typically associated with immunosuppression(47-51), produced unexpected results. At least two hypotheses can be proposed to explain these discrepancies. Initially, it is possible that we observed an off-target effect of alpelisib in mouse models and *ex vivo*. However, alpelisib is a potent and selective inhibitor of PI3Kα and the dosages employed in our experiments were extensively investigated and proven to have no impact on other isoforms(12, 47-52). Another explanation could be that in the context of inflammatory disorders like lupus, PI3Kα is upregulated and plays a significant role in cytokine production and the immune response.

In conclusion, our findings highlight that pharmacological inhibition of PI3Kα represents a very promising target for FSGS, lupus nephritis and more generally for proliferative glomerulonephritis.

Methods

Sex as a biological variant

In this study, sex was considered a biological variable in two lupus nephritis models: *NZBWF1/OlaHsd* and *MRL/MpJ-Fas^{lpr}/J* mice. These models are known to exhibit a more pronounced incidence and severity of symptoms in females. For the *NZBWF1/OlaHsd* model, only females were used. In the *MRL/MpJ-Fas^{lpr}/J* model, only females were used for the survival experiment. However, in other studies involving *MRL/MpJ-Fas^{lpr}/J* mice and in all other mouse models, both male and female mice were included. For human studies, both males and females were included, although the incidence of lupus is higher in females.

Animal studies

*R26StopFLP110** (Stock# 012343), *R26StopCAG-EGFP* (Stock# 006071), *Podocin Cre* mice (Stock# 008523), and *Podocin-iCre* mice on the *C57BL/6* background(53), *Tg26*/HIV mice (Stock# 022354) on *FVB* background, *Pik3Ca$^{lox/lox}$* mice (Stock# 017704), and MRL/MpJ-*Fas^{lpr}*/J (Stock# 000485) were obtained from Jackson Laboratory. *NZBWF1/OlaHsd* mice were obtained from Envigo. Whenever required, at least 10 backcrossings were conducted before using mice for experiments. Mice were randomly allocated to each experimental group in a sex-, age-, and body weight-matched manner, except when indicated otherwise. All animal procedures were approved by the *Ministère de l'Enseignement Supérieur, de la Recherche et de l'Innovation* (APAFIS N°20439-2018121913526398 and APAFIS N°30133-2020111914293579) and performed in accordance with the guidelines of Université Paris Cité to ensure animal welfare. For further details on mice experiments, please refer to the supplemental data.

Histopathology and immunohistochemistry analysis

The 4 µm paraffin-embedded kidney sections were stained with periodic acid-Schiff (PAS), Masson's Trichrome (MT), Periodic acid metenamine silver (PAM) or Hematoxylin and Eosin (HE) staining for histological analysis. The degree of glomerular lesions was evaluated using

the following scoring system: 0 = no lesion, 1 = affecting up to 25% of the glomerulus, 2 = affecting 25-50% of the glomerulus, 3 = affecting 50-75% of the glomerulus, and 4 = affecting 75-100%. At least 50 glomeruli per sample were measured for each analysis. An indirect immunoperoxidase method was used for immunohistochemistry. For further details, please refer to the supplemental data. The images were captured on a Zeiss LSM700 confocal microscope or Nikon AX confocal microscope. Immunohistochemistry revelation was performed with the appropriate horseradish peroxidase (HRP) antibodies and images were captured with a Nikon Eclipse E800 microscope. ImageJ software was used for analysis. Ilastik (interactive machine learning for (bio)image analysis, version 1.33post3) was used to select the positive signal area in the glomeruli, where its mean intensity for a target protein was measured.

Electron microscopy analysis

Small pieces of renal cortex (1 mm^3) were fixed in 2.5% glutaraldehyde solutions. For further sample process, please refer to the supplemental data. The prepared samples were examined in a JEOL 1011 transmission electron microscope (JEOL, Japan) with an ORIUS 1000 CCD camera (GATAN, France), operated with Digital Micrograph software (GATAN, France) for acquisition.

Mouse cell preparation and flow cytometry

Mononuclear cells (MNCs) from peripheral blood, spleen, bone marrow, and lymph nodes of mice treated with either the vehicle or alpelisib were prepared as described before(54). For further information, please refer to the supplemental material. Flow cytometry was performed using the Sony SP6800 Spectral Cell Analyzer, and data were analyzed with FlowJo software (TreeStar).

Preparation of the single-cell suspension

For imaging flow cytometry (Amnis ImageStream) or single-cell RNA-seq analysis, single-cell suspensions were prepared as follows. Euthanized mice were intravenously injected with M-450 Dynabeads (Thermo Fisher Scientific, ref# 14013) and saline. Kidneys were rinsed in phosphate-buffered saline and cut into small pieces in RPMI 1640 (Sigma-Aldrich) media on ice. Multi Tissue Dissociation Kit 1 (Miltenyi Biotec) was used for digesting the kidney. To enrich the glomeruli, kidney pieces were first stirred in the digestion buffer for 20 min at 37 degrees. Cells were then filtered (100 µm, Miltenyi Biotec) and centrifuged 5 min at 300 × *g* at 4 degrees. Cell pellets were resuspended in RPMI 1640 media and rinsed. The cell pellets were again resuspended in digestion buffer and digested with the half protocol 37C_Multi_B to make the single-cell suspension. Kidney cell suspensions were filtered (70 µm, Miltenyi Biotec), centrifuged 5 min at 300 × *g* at 4 degrees, and resuspended in RPMI 1640 media. Cell pellets were incubated with RBC lysis buffer (Miltenyi Biotec) on ice for 3 min, centrifuged at 300 × *g* for 5 min at 4 degrees, and resuspended in 1ml PBS + 0.04% BSA. Cell numbers and viability were analyzed under a microscope with a 0.4% Trypan Blue solution. The protocol was elaborated to minimize the experimental time to achieve the single-cell suspension with the maximum possible cell viability. For further scRNAseq and ImageStream experimental and analysis procedures, please refer to the supplemental material.

Human samples

Human samples were obtained from patients at Hôpital Necker Enfants Malades (Paris, France). Clinical and biological data that were available at the time of the kidney biopsy or lupus nephritis flare visit were collected. Classical histological and immunofluorescence analysis was performed with kidney biopsies fixed with formalin, alcohol, and acetic acid (AFA), which were subsequently embedded in paraffin. Some of the immunofluorescence studies and droplet digital PCR (ddPCR) were performed with OCT-frozen sections. Human peripheral blood mononuclear cells (PBMCs) and serum from lupus nephritis were obtained from flaring patients. PBMC were isolated from whole blood using a Ficoll-paque gradient. Written informed consent was obtained from each patient. Serum cytokines were measured with a V-PLEX®

proinflammatory panel 1 human kit (Meso Scale Discovery, MSD).

STAR-FISH and droplet digital PCR

STAR-FISH (Specific-To-Alele PCR – FISH) was performed as previously described(14). T-47D human breast tumor cell line (Sigma Aldrich) was cultured in DMEM (Sigma Aldrich) + 10% FCS (Sigma Aldrich). For droplet digital PCR (ddPCR), 20 µm frozen kidney sections were mounted on PEN-membrane slides (Leica) and rapidly stained with hematoxylin to recognize the kidney structure. Laser capture microdissection (LCM) was performed using a Leica LMD7000 system. Pools of glomeruli and tubules were collected for each patient. ddPCR (QX200 system, Bio-Rad Laboratories) was performed using the Mutation Detection Assay (FAM + HEX, Biorad Laboratories) to detect specifically the PIK3CA p.His1047Arg variant in the different pools, as previously described(55).

Spatial transcriptomics

GeoMx^{TM} digital spatial profiling experiments were performed according to the Nanostring GeoMx-NGS DSP instrument manual and as previously reported(56). Mouse anti-pan-cytokeratin (clone AE1/AE3, Novus Biologicals), rabbit anti-CD10 (clone EPR22867-118, Abcam), and mouse anti-CD31 (clone JC/70A, Abcam) were used as morphology markers. For further information, please refer to the supplemental material. Data analysis was performed on GeoMx DSP software v2.5.1.145. The Reactome database v78 was used for pathway analysis.

Data analysis and statistics

Data were expressed as the means ± SD. Survival curves were analyzed with the Log-rank (Mantel-Cox) test. Two-way ANOVA with Tukey's post hoc test, repeated-measures two-way ANOVA with Bonferroni's post hoc test, or the mixed-effects model with Bonferroni's post hoc test were used to determine the statistical significance between experimental groups. A two-tailed Student's t test, a two-tailed Mann-Whitney U test, or Wilcoxon matched-pairs signed

rank test was used to compare two-group experiments. One-way ANOVA with Tukey's post hoc test, or Friendman's test with Dunn's multiple comparisons test was used to compare one-group experiments. *P* value less than 0.05 was considered significant. The statistical analysis was performed using GraphPad Prism software (version 9.4.0).

Study approval

All animal procedures were approved by the Ministère de l'Enseignement Supérieur, de la Recherche et de l'Innovation (APAFIS N°20439-2018121913526398 and APAFIS N°30133-2020111914293579). The human studies were approved by the ethical committee (2021-A02719-32) and written informed consent was obtained from participants.

Data availability

The scRNA-Seq, and spatial transcriptomics have been deposited in the Gene Expression Omnibus (GEO) database (GSE263909 for the former and GSE264194 for the latter). All raw data are available in the Supporting Data Values file.

Acknowledgements: We'd like to thank Michaël Dussiot at the Institute Imagine for his assistance in imaging flow cytometry (Imagestream, Amnis), Nicolas Montcuquet at Sony Europe BV for his technical support in Sony ID7000 spectral analyzer, the histology platform at SFR Necker for histology services, and LEAT-Antenne at the Institute Imagine-SFR Necker for animal care. We also acknowledge *Région Ile-De-France* for the funding support of the Sony ID7000 spectral analyzer.

Funding: This study was supported by the European Research Council (CoG 2020 grant number 101000948 awarded to GC), the Agence Nationale de la Recherche – Programme d'Investissements d'Avenir (ANR-18-RHUS-005 to GC) and the Agence Nationale de la Recherche – Programme de Recherche Collaborative (19-CE14-0030-01 to GC). This work was also supported by the CLOVES SYNDROME COMMUNITY (West Kennebunk, USA), Association Syndrome de CLOVES (Nantes, France), Fondation d'entreprise IRCEM (Roubaix, France), Fondation Maladies Rares (Paris, France), Fonds de dotation Emmanuel BOUSSARD (Paris, France), the Fondation DAY SOLVAY (Paris, France), the Fondation TOURRE (Paris, France) to GC, the Fondation BETTENCOURT SCHUELLER (Paris, France) to GC, the Fondation Simone et Cino DEL DUCA (Paris, France), the Fondation Line RENAUD-Loulou GASTE (Paris, France), the Fondation Schlumberger pour l'Education et la Recherche (Paris, France), the Association Robert Debré pour la Recherche Médicale awarded to GC, WonderFIL smiles - a Facial Infiltrating Lipomatosis community (Norway), Fondation MSD Avenir (grant 'Signalopathies'), INSERM, Assistance Publique Hôpitaux de Paris and Université Paris Cité. We are also very grateful to our generous donors.

Author contributions: Junna Yamaguchi designed and evolved the study, performed most of the experiments, analyzed the data, elaborated figures and wrote the paper. Pierre Isnard analyzed human tissue sections, was involved in the spatial transcriptomic analysis and TEM analysis. Noémie Robil and Pierre de la Grange provided support for single-cell RNA sequencing analysis. Clément Hoguin was in charge of mice experiments including

genotyping, breeding, tamoxifen administration, nephrectomy and sacrifice. Aurélie Hummel identified lupus nephritis patients and was in charge of their follow-up. Alain Schmitt was involved in TEM images acquisition and analysis. Jérôme Megret provided help and support for flow cytometry experiments. Nicolas Goudin designed the algorithms for image analysis and quantification. Marine Luka, Mickael Menager, Cécile Masson, Mohamed Zarhrate and Christine Bôle-Feysot provided help and support for single-cell RNA sequencing experiments. Michalina Janiszewska and Kornelia Polyak performed the STAR-FISH PCR experiment. Julien Dairou performed the LC-MS analysis. Sara Baldassari and Stéphanie Baulac were involved in laser capture microdissection and droplet digital PCR. Christine Broissand was involved in the follow-up with patient 1. Christophe Legendre was involved in the follow-up with patient 1 and provided input for the manuscript. Fabiola Terzi provided input for the manuscript. Guillaume Canaud provided the conceptual framework, designed the study, supervised the project, elaborated figures and wrote the paper.

Competing interests:

- A patent application ("BYL719 (alpelisib) for use in the treatment of PIK3CA-related overgrowth spectrum" #WO2017140828A1) has been filed by INSERM (Institut National de la Santé et de la Recherche Médicale), Centre National de la Recherche Scientifique (CNRS), Université Paris Cité, and Assistance Publique-Hôpitaux de Paris (AP-HP) for the use of BYL719 (alpelisib) in the treatment of *PIK3CA*-related overgrowth spectrum (PROS/CLOVES syndrome). Dr. Canaud is the inventor. This patent is licensed to Novartis.
- A patent application ("Methods for the treatment of proliferative glomerulonephritis #EP22306011.2) has been filed by INSERM, CNRS, Université Paris Cité, and AP-HP. Dr. Canaud and Dr. Yamaguchi are the inventors.
- Dr. Canaud receives or has received consulting fees from Novartis, Vaderis, Alkermes, IPSEN and BridgeBio. The other authors declare that they have no competing interests.

References

1. Bilanges B, Posor Y, and Vanhaesebroeck B. PI3K isoforms in cell signalling and vesicle trafficking. *Nature reviews Molecular cell biology.* 2019.
2. Welch HC, Coadwell WJ, Stephens LR, and Hawkins PT. Phosphoinositide 3-kinase-dependent activation of Rac. *FEBS Lett.* 2003;546(1):93-7.
3. Kurek KC, Luks VL, Ayturk UM, Alomari AI, Fishman SJ, Spencer SA, et al. Somatic mosaic activating mutations in PIK3CA cause CLOVES syndrome. *American journal of human genetics.* 2012;90(6):1108-15.
4. Keppler-Noreuil KM, Sapp JC, Lindhurst MJ, Parker VE, Blumhorst C, Darling T, et al. Clinical delineation and natural history of the PIK3CA-related overgrowth spectrum. *Am J Med Genet A.* 2014;164A(7):1713-33.
5. Keppler-Noreuil KM, Rios JJ, Parker VE, Semple RK, Lindhurst MJ, Sapp JC, et al. PIK3CA-related overgrowth spectrum (PROS): diagnostic and testing eligibility criteria, differential diagnosis, and evaluation. *Am J Med Genet A.* 2015;167A(2):287-95.
6. Luks VL, Kamitaki N, Vivero MP, Uller W, Rab R, Bovee JV, et al. Lymphatic and other vascular malformative/overgrowth disorders are caused by somatic mutations in PIK3CA. *The Journal of pediatrics.* 2015;166(4):1048-54 e1-5.
7. Mirzaa GM, Conway RL, Gripp KW, Lerman-Sagie T, Siegel DH, deVries LS, et al. Megalencephaly-capillary malformation (MCAP) and megalencephaly-polydactyly-polymicrogyria-hydrocephalus (MPPH) syndromes: two closely related disorders of brain overgrowth and abnormal brain and body morphogenesis. *Am J Med Genet A.* 2012;158A(2):269-91.

8. Rios JJ, Paria N, Burns DK, Israel BA, Cornelia R, Wise CA, et al. Somatic gain-of-function mutations in PIK3CA in patients with macrodactyly. *Human molecular genetics.* 2013;22(3):444-51.

9. Rivière JB, Mirzaa GM, O'Roak BJ, Beddaoui M, Alcantara D, Conway RL, et al. De novo germline and postzygotic mutations in AKT3, PIK3R2 and PIK3CA cause a spectrum of related megalencephaly syndromes. *Nature genetics.* 2012;44(8):934-40.

10. Morin GM, Zerbib L, Kaltenbach S, Fraissenon A, Balducci E, Asnafi V, et al. PIK3CA-Related Disorders: From Disease Mechanism to Evidence-Based Treatments. *Annu Rev Genomics Hum Genet.* 2024.

11. Venot Q, Blanc T, Rabia SH, Berteloot L, Ladraa S, Duong JP, et al. Targeted therapy in patients with PIK3CA-related overgrowth syndrome. *Nature.* 2018;558(7711):540-6.

12. Fritsch C, Huang A, Chatenay-Rivauday C, Schnell C, Reddy A, Liu M, et al. Characterization of the novel and specific PI3Kalpha inhibitor NVP-BYL719 and development of the patient stratification strategy for clinical trials. *Molecular cancer therapeutics.* 2014;13(5):1117-29.

13. Canaud G, Bienaime F, Viau A, Treins C, Baron W, Nguyen C, et al. AKT2 is essential to maintain podocyte viability and function during chronic kidney disease. *Nature medicine.* 2013.

14. Janiszewska M, Liu L, Almendro V, Kuang Y, Paweletz C, Sakr RA, et al. In situ single-cell analysis identifies heterogeneity for PIK3CA mutation and HER2 amplification in HER2-positive breast cancer. *Nature genetics.* 2015;47(10):1212-9.

15. Muzumdar MD, Tasic B, Miyamichi K, Li L, and Luo L. A global double-fluorescent Cre reporter mouse. *Genesis.* 2007;45(9):593-605.

16. Barisoni L, Bruggeman LA, Mundel P, D'Agati VD, and Klotman PE. HIV-1 induces renal epithelial dedifferentiation in a transgenic model of HIV-associated nephropathy. *Kidney international.* 2000;58(1):173-81.

17. Griffin SV, Petermann AT, Durvasula RV, and Shankland SJ. Podocyte proliferation and differentiation in glomerular disease: role of cell-cycle regulatory proteins. *Nephrol Dial Transplant.* 2003;18 Suppl 6:vi8-13.

18. Park J, Shrestha R, Qiu C, Kondo A, Huang S, Werth M, et al. Single-cell transcriptomics of the mouse kidney reveals potential cellular targets of kidney disease. *Science (New York, NY.* 2018;360(6390):758-63.

19. Bukosza EN, Kratochwill K, Kornauth C, Schachner H, Aufricht C, and Gebeshuber CA. Podocyte RNA sequencing reveals Wnt- and ECM-associated genes as central in FSGS. *PLoS One.* 2020;15(4):e0231898.

20. Albaqumi M, Soos TJ, Barisoni L, and Nelson PJ. Collapsing glomerulopathy. *J Am Soc Nephrol.* 2006;17(10):2854-63.

21. Bomback AS, and Markowitz GS. Lupus Podocytopathy: A Distinct Entity. *Clinical journal of the American Society of Nephrology : CJASN.* 2016;11(4):547-8.

22. Rednor SJ, and Ross MJ. Molecular Mechanisms of Injury in HIV-Associated Nephropathy. *Front Med (Lausanne).* 2018;5:177.

23. Shah SN, He CJ, and Klotman P. Update on HIV-associated nephropathy. *Current opinion in nephrology and hypertension.* 2006;15(4):450-5.

24. Rosenberg AZ, Naicker S, Winkler CA, and Kopp JB. HIV-associated nephropathies: epidemiology, pathology, mechanisms and treatment. *Nature reviews Nephrology.* 2015;11(3):150-60.

25. Kopp JB, Klotman ME, Adler SH, Bruggeman LA, Dickie P, Marinos NJ, et al. Progressive glomerulosclerosis and enhanced renal accumulation of basement membrane components in mice transgenic for human immunodeficiency virus type 1 genes. *Proceedings of the National Academy of Sciences of the United States of America.* 1992;89(5):1577-81.

26. Celhar T, and Fairhurst AM. Modelling clinical systemic lupus erythematosus: similarities, differences and success stories. *Rheumatology (Oxford).* 2017;56(suppl_1):i88-i99.

27. Vanhaesebroeck B, Welham MJ, Kotani K, Stein R, Warne PH, Zvelebil MJ, et al. P110delta, a novel phosphoinositide 3-kinase in leukocytes. *Proceedings of the National Academy of Sciences of the United States of America.* 1997;94(9):4330-5.

28. Ramadani F, Bolland DJ, Garcon F, Emery JL, Vanhaesebroeck B, Corcoran AE, et al. The PI3K isoforms p110alpha and p110delta are essential for pre-B cell receptor signaling and B cell development. *Science signaling.* 2010;3(134):ra60.

29. Okkenhaug K, Patton DT, Bilancio A, Garcon F, Rowan WC, and Vanhaesebroeck B. The p110delta isoform of phosphoinositide 3-kinase controls clonal expansion and differentiation of Th cells. *J Immunol.* 2006;177(8):5122-8.

30. Soond DR, Bjorgo E, Moltu K, Dale VQ, Patton DT, Torgersen KM, et al. PI3K p110delta regulates T-cell cytokine production during primary and secondary immune responses in mice and humans. *Blood.* 2010;115(11):2203-13.

31. Lewis DE, Giorgi JV, and Warner NL. Flow cytometry analysis of T cells and continuous T-cell lines from autoimmune MRL/l mice. *Nature.* 1981;289(5795):298-300.

32. Watson ML, Rao JK, Gilkeson GS, Ruiz P, Eicher EM, Pisetsky DS, et al. Genetic analysis of MRL-lpr mice: relationship of the Fas apoptosis gene to disease manifestations and renal disease-modifying loci. *J Exp Med.* 1992;176(6):1645-56.

33. Furukawa F, Kanauchi H, Wakita H, Tokura Y, Tachibana T, Horiguchi Y, et al. Spontaneous autoimmune skin lesions of MRL/n mice: autoimmune disease-prone genetic background in relation to Fas-defect MRL/1pr mice. *The Journal of investigative dermatology.* 1996;107(1):95-100.

34. Madsen RR. PI3K in stemness regulation: from development to cancer. *Biochemical Society transactions.* 2020;48(1):301-15.

35. Yu JS, and Cui W. Proliferation, survival and metabolism: the role of PI3K/AKT/mTOR signalling in pluripotency and cell fate determination. *Development (Cambridge, England).* 2016;143(17):3050-60.

36. Vadlakonda L, Pasupuleti M, and Pallu R. Role of PI3K-AKT-mTOR and Wnt Signaling Pathways in Transition of G1-S Phase of Cell Cycle in Cancer Cells. *Front Oncol.* 2013;3:85.

37. Dai C, Stolz DB, Kiss LP, Monga SP, Holzman LB, and Liu Y. Wnt/beta-catenin signaling promotes podocyte dysfunction and albuminuria. *J Am Soc Nephrol.* 2009;20(9):1997-2008.

38. Kato H, and Susztak K. Repair problems in podocytes: Wnt, Notch, and glomerulosclerosis. *Seminars in nephrology.* 2012;32(4):350-6.

39. Shkreli M, Sarin KY, Pech MF, Papeta N, Chang W, Brockman SA, et al. Reversible cell-cycle entry in adult kidney podocytes through regulated control of telomerase and Wnt signaling. *Nature medicine.* 2012;18(1):111-9.

40. Fioretto P, Steffes MW, Sutherland DE, Goetz FC, and Mauer M. Reversal of lesions of diabetic nephropathy after pancreas transplantation. *The New England journal of medicine.* 1998;339(2):69-75.

41. Puelles VG, van der Wolde JW, Wanner N, Scheppach MW, Cullen-McEwen LA, Bork T, et al. mTOR-mediated podocyte hypertrophy regulates glomerular integrity in mice and humans. *JCI Insight.* 2019;4(18).

42. Mallipattu SK, and He JC. The podocyte as a direct target for treatment of glomerular disease? *Am J Physiol Renal Physiol.* 2016;311(1):F46-51.

43. Fantus D, Rogers NM, Grahammer F, Huber TB, and Thomson AW. Roles of mTOR complexes in the kidney: implications for renal disease and transplantation. *Nature reviews Nephrology.* 2016;12(10):587-609.

44. Canaud G, Bienaime F, Tabarin F, Bataillon G, Seilhean D, Noel LH, et al. Inhibition of the mTORC pathway in the antiphospholipid syndrome. *The New England journal of medicine.* 2014;371(4):303-12.

45. Johnson SC, Martinez F, Bitto A, Gonzalez B, Tazaerslan C, Cohen C, et al. mTOR inhibitors may benefit kidney transplant recipients with mitochondrial diseases. *Kidney international.* 2018.

46. Bissler JJ, Kingswood JC, Radzikowska E, Zonnenberg BA, Frost M, Belousova E, et al. Everolimus for angiomyolipoma associated with tuberous sclerosis complex or sporadic lymphangioleiomyomatosis (EXIST-2): a multicentre, randomised, double-blind, placebo-controlled trial. *Lancet.* 2013;381(9869):817-24.

47. Andre F, Ciruelos E, Rubovszky G, Campone M, Loibl S, Rugo HS, et al. Alpelisib for PIK3CA-Mutated, Hormone Receptor-Positive Advanced Breast Cancer. *The New England journal of medicine.* 2019;380(20):1929-40.

48. Vanhaesebroeck B, Perry MWD, Brown JR, Andre F, and Okkenhaug K. PI3K inhibitors are finally coming of age. *Nat Rev Drug Discov.* 2021.

49. Delestre F, Venot Q, Bayard C, Fraissenon A, Ladraa S, Hoguin C, et al. Alpelisib administration reduced lymphatic malformations in a mouse model and in patients. *Science translational medicine.* 2021;13(614):eabg0809.

50. Ladraa S, Zerbib L, Bayard C, Fraissenon A, Venot Q, Morin G, et al. PIK3CA gain-of-function mutation in adipose tissue induces metabolic reprogramming with Warburg-like effect and severe endocrine disruption. *Sci Adv.* 2022;8(49):eade7823.

51. Morin G, Degrugillier-Chopinet C, Vincent M, Fraissenon A, Aubert H, Chapelle C, et al. Treatment of two infants with PIK3CA-related overgrowth spectrum by alpelisib. *J Exp Med.* 2022;219(3).

52. Furet P, Guagnano V, Fairhurst RA, Imbach-Weese P, Bruce I, Knapp M, et al. Discovery of NVP-BYL719 a potent and selective phosphatidylinositol-3 kinase alpha inhibitor selected for clinical evaluation. *Bioorganic & medicinal chemistry letters.* 2013;23(13):3741-8.

53. Mollet G, Ratelade J, Boyer O, Muda AO, Morisset L, Lavin TA, et al. Podocin inactivation in mature kidneys causes focal segmental glomerulosclerosis and nephrotic syndrome. *J Am Soc Nephrol.* 2009;20(10):2181-9.

54. Kobayashi H, Morikawa T, Okinaga A, Hamano F, Hashidate-Yoshida T, Watanuki S, et al. Environmental Optimization Enables Maintenance of Quiescent Hematopoietic Stem Cells Ex Vivo. *Cell Rep.* 2019;28(1):145-58 e9.

55. Baldassari S, Ribierre T, Marsan E, Adle-Biassette H, Ferrand-Sorbets S, Bulteau C, et al. Dissecting the genetic basis of focal cortical dysplasia: a large cohort study. *Acta Neuropathol.* 2019;138(6):885-900.

56. Merritt CR, Ong GT, Church SE, Barker K, Danaher P, Geiss G, et al. Multiplex digital spatial profiling of proteins and RNA in fixed tissue. *Nature biotechnology.* 2020;38(5):586-99.

Figure legends

Figure 1: *PIK3CA* gain-of-function mutation in podocytes leads to severe glomerular disease. (**A**-**C**) Patient 1 kidney. (**A**) Trichrome and PAS staining. Black arrow showing hypercellularity. Red arrow showing hypertrophy and hyperplasia of the overlying podocytes. (**B**) P-AKT^{Ser473} or P-S6RP coimmunofluorescence staining with Nephrin. (**C**) In situ *H1047 PIK3CA* hybridization. Yellow dots contour glomerulus. Red dots are mutation positive points. (**D**, **E**) Urinary albumin to creatinine ratio, serum creatinine and BUN of *PIK3CA*^{WT} and *PIK3CA*$^{Pod\text{-}HET}$ mice with ageing. 3-m.o. *PIK3CA*^{WT}, n=5, 3-m.o. *PIK3CA*^{HET}, n=6, 6-m.o. *PIK3CA*^{WT}, n=6, 6-m.o. *PIK3CA*^{HET}, n=6, 12-m.o. *PIK3CA*^{WT}, n=6, 12-m.o. *PIK3CA*^{HET}, n=8. (**F**) Kaplan-Meier curves of *PIK3CA*^{WT} (n=27), *PIK3CA*$^{Pod\text{-}HET}$ (n=12), and *PIK3CA*$^{Pod\text{-}HO}$ mice (n=28). (**G**-**M**) 5-month-old *PIK3CA*^{WT} and *PIK3CA*$^{Pod\text{-}HET}$ mice kidneys. (**G**) PAS and glomerular sclerosis (GS) index quantification (n=5 mice per group). (**H**) P-S6RP and P-AKT^{Ser473} immunofluorescence staining. (**I**) Glomerular P-S6RP, P-AKT^{Ser473} and P-AKT^{Thr308} quantification (n=5 mice per group). (**J-M**) Representative WT1 or Ki-67 immunostaining and quantification (n=6 mice per group). (**N**) Amnis ImageStream analysis of podocytes of 4-month-old *PIK3CA*^{WT} and *PIK3CA*$^{Pod\text{-}HET}$ mice (n=3 per group). (**O**) Coomassie blue staining of *PIK3CA*^{WT}, *PIK3CA*$^{Pod\text{-}HET}$ and *PIK3CA*$^{Pod\text{-}HO}$ mice. Values are means ± SD. *P* values calculated using two-way ANOVA with Tukey's post hoc test (**D**, **E**); Log-rank (Mantel-Cox) test (**F**); two-tailed Mann-Whitney U test (**I**); or two-tailed *t* test (**G**, **K**, **M**, **N**). Scale bars: 100 μm (Trichrome) and 40 μm (PAS) (**A**), 20 μm (**B**, **H**), 25 μm (**G**), 32.2 μm (**J**, **L**).

Figure 2: *PIK3CA* gain-of-function mutation in podocytes is associated with changes in cell fate determination. (**A**) Unsupervised clustering resulted in 20 distinct cell types in the UMAP map. (**B**) Expression of cell-type specific markers to annotate clusters. The cell percentage expressing the gene is expressed by the dot's size, and the average expression of the gene is expressed by the color concentration. (**C**) Cell trajectory map of each podocyte cluster showing the pseudo-time. The significant pathways resulting from the KEGG pathway analysis are displayed adjacent to clusters of podocytes 1, 2, and 3.

Figure 3: Alpelisib modifies podocyte cell fate determination in *PIK3CA*$^{Pod\text{-}HET}$ mice.

(**A**) Histogram showing the distribution of podocyte cluster (1-6) cells along pseudo-time for each sample. *PIK3CA*$^{Pod\text{-}HET}$-vehicle mice podocytes show a distinct distribution. (**B**) UMAP plot per sample showing the populational change for podocyte clusters. The podocyte clusters (1-6) are indicated by dotted lines that encompass their respective percentages of total cells in each sample.

Figure 4: Alpelisib improves kidney lesions in uninephrectomized *PIK3CA*$^{Pod\text{-}HO}$ mice. (**A**) Experimental protocol design. UNx: Uninephrectomy. (**B**-**M**) n=8 for *PIK3CA*^{WT}-Vehicle, *PIK3CA*^{WT}-Alpelisib, *PIK3CA*^{HO}-Vehicle, and n=9 for *PIK3CA*^{HO}-Alpelisib, unless otherwise stated. (**B**, **C**) Urinary albumin/creatinine ratio, or BUN of *PIK3CA*^{WT} and *PIK3CA*$^{Pod\text{-}HO}$ mice at sacrifice (2 weeks Tx following UNx). (**D**) Representative PAS staining of UNx kidneys from *PIK3CA*^{WT} and *PIK3CA*$^{Pod\text{-}HO}$ mice. (**E**-**K**) Kidneys from *PIK3CA*^{WT} and *PIK3CA*$^{Pod\text{-}HO}$ mice at sacrifice. (**E**) PAS staining and (**F**) GS index. (**G**) P-AKT^{Ser473} immunofluorescence staining and (**H**) P-AKT^{Ser473} quantification of glomeruli (n=5 mice per group). (**I**) P-S6RP/Nephrin coimmunofluorescence staining, and their glomerular quantification (**J** and **K**) (n=5 mice per group). (**L**) Trajectory of the albumin to creatinine ratio in the urine, and (**M**) trajectory of GS index of *PIK3CA*$^{Pod\text{-}HO}$ mice following UNx and treated with either vehicle or alpelisib. Data are represented as means ± SD from 3 independent experiments for **B**, **C**, **F**, **L**, **M**), and means ± SD and representative of 3 independent experiments (**H**, **J**, **K**). P values are calculated using two-way ANOVA with Tukey's post hoc test (**B**, **C**, **F**, **H**, **J**, and **K**); Wilcoxon matched-pairs signed rank test (**L**), and two- way ANOVA with Bonferroni's multiple comparison test (**M**). Scale bars: 32.2 μm (**D**, **E**), 20 μm (**G**, **I**). Some data are identical between (**B**) and (**L**).

Figure 5: Spatial transcriptomic changes observed in glomeruli from patients with class 4 lupus nephritis. (**A**) Representative coimmunofluorescence staining of Nephrin/P-AKT^{Ser473} (frozen section) and Nephrin/P-S6RP in kidney biopsies from patients with lupus nephritis (LN), ANCA vasculitis or controls (n=4 patients per group). (**B**) Glomerular P-AKT^{Ser473} and P-S6RP

quantification (n=4 patients per group). (**C**) GSEA mapping from the reactome for LN vs. controls. Some of the pathways of interest that are enriched in LN samples are highlighted in colored dots as follows: inflammation related in yellow, metabolism related in magenta, pluripotency related in orange, extracellular matrix organization related in green, DNA replication and protein translation related in light blue, and PI3K-AKT signaling pathway related in navy blue. (**D**) Volcano plot between controls and LN samples. Significantly differentially expressed genes are colored with red dots. (**E**) Bar plot of the top normalized enriched score-ranked gene sets (hallmark, GSEA) with $p< 0.001$ in LN pAKT activity-high kidneys compared with LN pAKT activity-low ROIs. (**F**) Volcano plot between the LN pAKT activity-high and LN pAKT activity-low ROIs. Significantly differentially expressed genes are colored with red dots. Data are represented as means ± SD, and P values calculated using one-way ANOVA with Tukey's post hoc test (**B**). Scaler bars: 20 μm (**A**).

Figure 6: Alpelisib improves kidney lesions in an accelerated mouse model of collapsing glomerulopathy. (**A**) Experimental protocol design. (**B**-**M**) *Tg26*^{WT} and *Tg26*^{He} mice at the time of sacrifice (n= 16 for *Tg26*^{WT}-Vehicle, n= 15 for *Tg26*^{WT}-Alpelisib, n=18 for *Tg26*^{He}-Vehicle, n=19 for *Tg26*^{He}-Alpelisib, except otherwise stated). (**B**) Serum creatinine, (**C**) BUN, (**D**) urinary albumin-to-creatinine ratio, (**E**) representative PAS staining of kidneys, (**F**) GS index quantification, and (**G**) representative Nephrin immunofluorescence staining of kidneys. (**H**) Representative P-AKT^{Ser473} immunofluorescence and their glomerular quantification (**I**) from *Tg26*^{WT} and *Tg26*^{He} mice kidney at sacrifice (n= 6 mice per group). (**J**) The urinary albumin-to-creatinine ratio trajectory of *Tg26*^{WT} and *Tg26*^{He} mice following UNx and Tx. (**K**) GS index trajectory between UNx and sacrifice kidneys of *Tg26*^{He} mice. (**L**) BUN, (**M**) Serum creatinine level trajectory of *Tg26*^{WT} and *Tg26*^{He} mice following UNx and Tx. Data are represented as means ± SD are from 6 independent experiments (**B-F**, **J-M**), or are means ± SD and representative of 3 independent experiments (**H**-**I**). P values calculated using two-way ANOVA with Tukey's post hoc test (**B**-**D**, **F**, **I**); two-way ANOVA with Bonferroni's multiple

comparisons test (**J**-**M**). Scale bars: 130 μm (**E** upper), 32.2 μm (**E** lower), 20 μm (**G**, **H**). Note some data are shared between (**B**) and (**M**), (**C**) and (**L**), (**D**) and (**J**), (**G**) and (**K**).

Figure 7: *PIK3CA* deletion in podocytes improves kidney lesions in an accelerated mouse model of collapsing glomerulopathy. (**A**-**G**) 15-week-old *Tg26*^{WT}-*PIK3CA*$^{Podo\text{-}WT}$ (n=18), *Tg26*^{WT}-*PIK3CA*$^{Podo\text{-}KO}$ (n=14), *Tg26*^{He}-*PIK3CA*$^{Podo\text{-}WT}$ (n=15), and *Tg26*^{He}-*PIK3CA*$^{Podo\text{-}KO}$ mice (n=15). (**A**) Urinary albumin to creatinine ratio, (**B**) Serum creatinine level, (**C**) BUN level, (**D**) Kidney-to-body weight ratio, (**E**) Spleen to body weight ratio, (**F**) Representative PAS staining of kidneys, and (**G**) GS index quantification. (**H**) *Col1a*, (**I**) *Col3a*, (**J**) *Kim1*, (**K**) Lcn2, and (**L**) *Tnfα* quantification of qRT-PCR analysis in the kidney cortex from 15-week-old *Tg26*^{WT}-*PIK3CA*$^{Podo\text{-}WT}$ (n=7), *Tg26*^{WT}-*PIK3CA*$^{Podo\text{-}KO}$ (n=3), *Tg26*^{He}-*PIK3CA*$^{Podo\text{-}WT}$ (n= 6) and *Tg26*^{He}-*PIK3CA*$^{Podo\text{-}KO}$ mice (n=6). Data are represented as means ± SD from at least 3 independent experiments (**A**-**E**, **G**-**L**). P values calculated using two-way ANOVA with Tukey's post hoc test (**A**-**E**, **G**-**L**). Scale bars: 130 μm (**F** upper), 32.2 μm (**F** lower).

Figure 8: *PIK3CA* deletion in podocytes up to the age of 6 weeks is able to reverse kidney lesions in *Tg26* mice. (**A**) Representative PAS staining of the kidneys at 12 weeks from *Tg26*^{He} with either *PIK3CA*$^{iPodo\text{-}WT}$ or *PIK3CA*$^{iPodo\text{-}KO}$ mice, which were induced with tamoxifen at different time points (3 weeks old *Tg26*^{WT}-*PIK3CA*$^{iPodo\text{-}WT}$, n=10, 3 weeks old *Tg26*^{WT}-*PIK3CA*$^{iPodo\text{-}KO}$, n=8, 3 weeks old *Tg26*^{He}-*PIK3CA*$^{iPodo\text{-}WT}$, n=14, 3 weeks old *Tg26*^{He}-*PIK3CA*$^{iPodo\text{-}KO}$, n=11, 6 weeks old *Tg26*^{WT}-*PIK3CA*$^{iPodo\text{-}WT}$, n=10, 6 weeks old *Tg26*^{WT}-*PIK3CA*$^{iPodo\text{-}KO}$, n=14, 6 weeks old *Tg26*^{He}-*PIK3CA*$^{iPodo\text{-}WT}$, n=16, 6 weeks old *Tg26*^{He}-*PIK3CA*$^{iPodo\text{-}KO}$, n=14, 8 weeks old *Tg26*^{WT}-*PIK3CA*$^{iPodo\text{-}WT}$, n=10, 8 weeks old *Tg26*^{WT}-*PIK3CA*$^{iPodo\text{-}KO}$, n=11, 8 weeks old *Tg26*^{He}-*PIK3CA*$^{iPodo\text{-}WT}$, n=14, 8 weeks old *Tg26*^{He}-*PIK3CA*$^{iPodo\text{-}KO}$, n=16). (**B**-**D**) GS index quantification, and the urinary albumin to creatinine ratio of mice that were induced at indicated time points. Data are represented as means ± SD from at least 3 independent experiments (**B**-**D**). P values calculated using two-way ANOVA with

Tukey's post hoc test (**B** right, **C** right), and two-tailed *t* test (**B** left, **C** left, and **D**). Scale bars: 100 μm (**A**).

Figure 9: Alpelisib improves kidney lesions in *NZBWF1/J* lupus nephritis models. (**A**-**J**) *NZBWF1/J* at sacrifice except otherwise stated (Sham-Vehicle and Sham-Alpelisib, n=5, UNx-Vehicle and UNx-Alpelisib, n=15). (**A**) Urinary albumin-to-creatinine ratio, (**B**) BUN, (**C**) Kidney-to-body weight ratio, (**D**) Representative PAS staining, (**E**) GS index quantification at sacrifice, GS trajectory between UNx and sacrifice of the same mouse. GS at sacrifice shared. (**F**) Representative P-S6RP/Nephrin coimmunofluorescence staining, (**G**) quantification (n=6 per group). (**H**) *Col3a*, (**I**) *Col1a*, and (**J**) *Tnfα* quantification of qRT-PCR in kidney cortex. (**K**) Western blot and quantification of Nephrin, Podocin, and α-tubulin in kidney cortex (UNx-Vehicle, n=6, UNx-Alpelisib, n=7). (**L**) IgG, (**M**) IgM, and (**N**) C3 raw intensity per glomerulus quantification of the immunofluorescence staining (UNx-Vehicle, n=6, UNx-Alpelisib, n=7). Data represented as means ± SD, 3 independent experiments (**A-C**, **E**, **G-N**). P values calculated using two-way ANOVA with Tukey's post hoc test (**A**-**C G**-**J**); two-way ANOVA with Bonferroni's multiple comparisons test (**E** right), two-tailed *t* test (**E** left and **K**), two-tailed Mann-Whitney U test (**L**-**N**). Scale bar 130μm (**D** upper), 32.2μm (**D** lower), 20μm (**F**).

Figure 10: Alpelisib improves kidney lesions in *MRL-lpr* lupus nephritis models. (**A**-**J**) *MRL-lpr* mice survival experiment (Vehicle, n=13, Alpelisib, n=14, except otherwise stated). (**A**) Kaplan-Meier curves, (**B**) Urinary albumin-to-creatinine ratio at sacrifice, (**C**, **D**) Trajectory of urinary albumin-to-creatinine ratio (After Tx are same as **B**), (**E**) Kidney-to-body weight, (**F**) Spleen-to-body weight, (**G**) Representative PAS staining**,** (**H**) GS index quantification (n=8 per group), (**I**) Serum creatinine and (**J**) BUN at sacrifice. (**K**-**T**) *MRL-lpr* treated either with vehicle or alpelisib from 12 until 16 weeks old (n=6 per group except otherwise stated). (**K**) Representative PAS staining, (**L**) GS index quantification, (**M**) *Col1a* and (**N**) *Col3a* quantification of qRT-PCR in kidney cortex (n=14 per group). (**O**) Representative P-

S6RP/Nephrin, (**P**) P-AKT^{Ser473} immunofluorescence staining, and (**Q**, **R**) their quantification. (**S**) Western blot and quantification of Nephrin, Podocin, P-S6RP, S6RP, and α-tubulin in kidney cortex. (**T**) Serum dsDNA titer changes ratio (after-Tx to before-Tx) (Vehicle, n=12, Alpelisib, n=13). Data represented as means ± SD, 3 independent experiments (**B**, **E**, **F**, **H**-**J**, **L**-**N**, **Q**-**T**). P values calculated using Log-rank (Mantel-Cox) test (**A**), two-tailed *t* test (**E**, **F**, **I**, **J**, **L**, and **S**), Wilcoxon matched-pairs signed rank test (**C** and **D**), two-tailed Mann-Whitney U test (**B**, **H**, **M**, **N**, **Q**, **R**, and **T**). Scale bars 100μm (**G**, **K**), 20μm (**O**, **P**).

Figure 11: Alpelisib impaired, in vitro, B and T cell activation from lupus patients. (**A**) P-S6RP intensity at day 1 in CD19+ B cells from 4 patients with active lupus nephritis (LN1-4) following stimulation and treated with vehicle or alpelisib 5μM. LN1 unstimulated (n=687 cells), LN1 stimulated (n=1031 cells), LN1 stimulated + alpelisib (n=668 cells), LN2 unstimulated (n=6059 cells), LN2 stimulated (n=7289 cells), LN2 stimulated + alpelisib (n=7533 cells), LN3 unstimulated (n=2623 cells), LN3 stimulated (n=2442 cells), LN3 stimulated + alpelisib (n=2161 cells), LN4 unstimulated (n=12542 cells), LN4 stimulated (n=9224 cells), LN4 stimulated + alpelisib (n=29800 cells). (**B**) P-S6RP intensity and CD69 population at day 1 in CD3+ T cells from LN1-4 following stimulation and treated with vehicle or alpelisib. LN1 unstimulated (n=14521 cells), LN1 stimulated (n=5047 cells), LN1 stimulated + alpelisib 5μM (n=6589 cells), LN1 stimulated + alpelisib 10μM (n=7834 cells), LN2 unstimulated (n=18284 cells), LN2 stimulated (n=8106 cells), LN2 stimulated + alpelisib 5μM (n=10208 cells), LN2 stimulated + alpelisib 10μM (n=13758 cells), LN3 unstimulated (n=9066 cells), LN3 stimulated (n=6176 cells), LN3 stimulated + alpelisib 5μM (n=6707 cells), LN3 stimulated + alpelisib 10μM (n=6570 cells), LN4 unstimulated (n=12542 cells), LN4 stimulated (n=9224 cells), LN4 stimulated + alpelisib 5μM (n=29800 cells), LN4 stimulated + alpelisib 10μM (n=27863 cells). (**C**) Cytokine measurements at day 7 in supernatant from non-stimulated or stimulated CD3+ T cells, treated with the vehicle or 5μM or 10μM alpelisib. Patients LN1-4 are included in the analysis. IFN-γ, TNF-α, and IL-1β are shown here. Means ± SD. P values calculated using

one-way ANOVA with Tukey's post hoc test (**A**, **B**), and Friedman test with Dunn's multiple comparisons test (**C**).

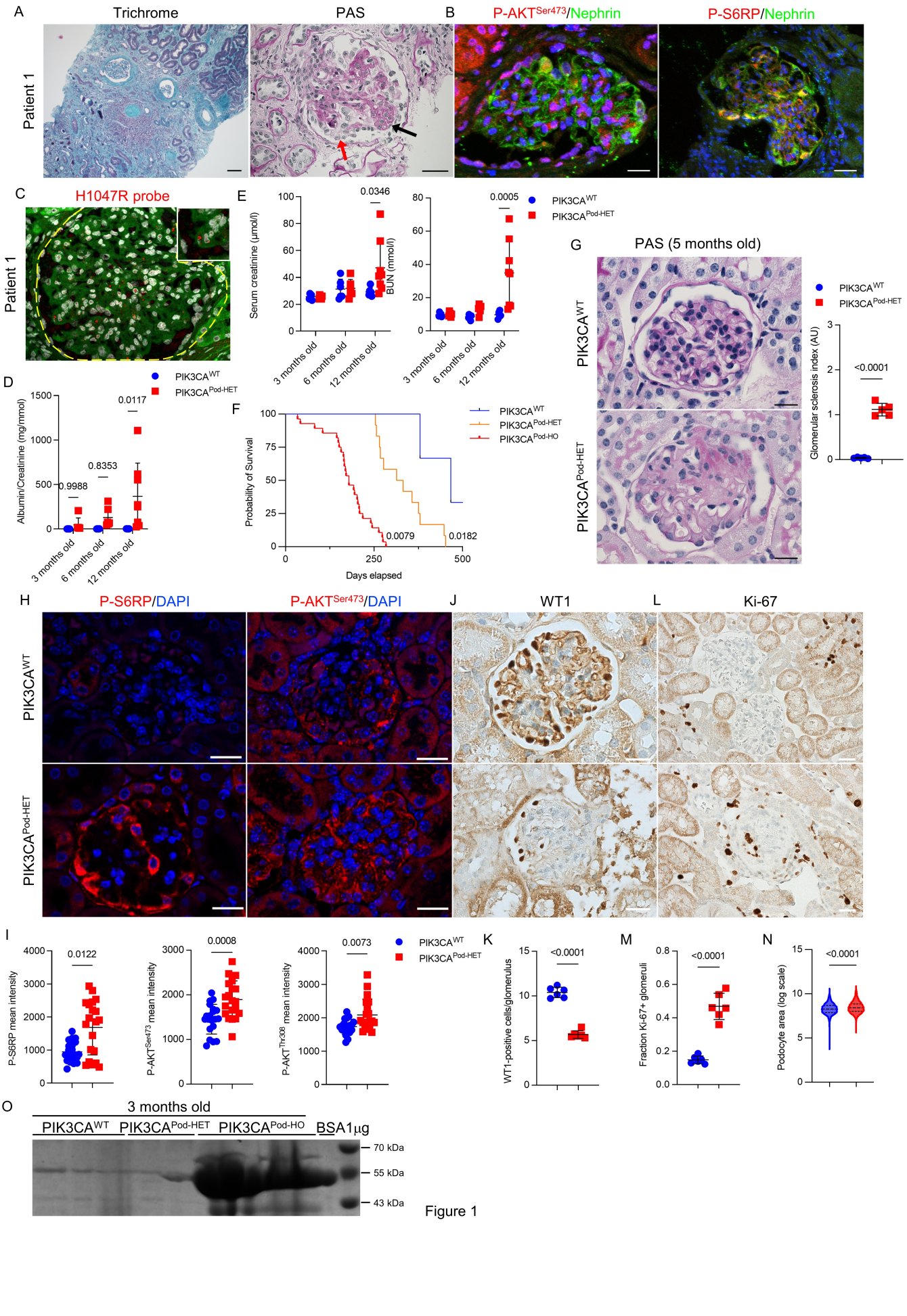
A
Trichrome
PAS
Patient 1
B
P-AKTSer473/Nephrin
P-S6RP/Nephrin
C
H1047R probe
Patient 1
D
PIK3CAWT
PIK3CAPod-HET
Albumin/Creatinine (mg/mmol)
0.9988
0.8353
0.0117
3 months old
6 months old
12 months old
E
Serum creatinine (µmol/l)
BUN (mmol/l)
0.0346
0.0005
PIK3CAWT
PIK3CAPod-HET
F
PIK3CAWT
PIK3CAPod-HET
PIK3CAPod-HO
Probability of Survival
0.0079
0.0182
Days elapsed
G
PAS (5 months old)
PIK3CAWT
PIK3CAPod-HET
Glomerular sclerosis index (AU)
<0.0001
H
P-S6RP/DAPI
P-AKTSer473/DAPI
PIK3CAWT
PIK3CAPod-HET
J
WT1
L
Ki-67
I
P-S6RP mean intensity
P-AKTSer473 mean intensity
P-AKTThr308 mean intensity
0.0122
0.0008
0.0073
PIK3CAWT
PIK3CAPod-HET
K
WT1-positive cells/glomerulus
<0.0001
M
Fraction Ki-67+ glomeruli
<0.0001
N
Podocyte area (log scale)
<0.0001
O
3 months old
PIK3CAWT
PIK3CAPod-HET
PIK3CAPod-HO
BSA1µg
70 kDa
55 kDa
43 kDa

Figure 1

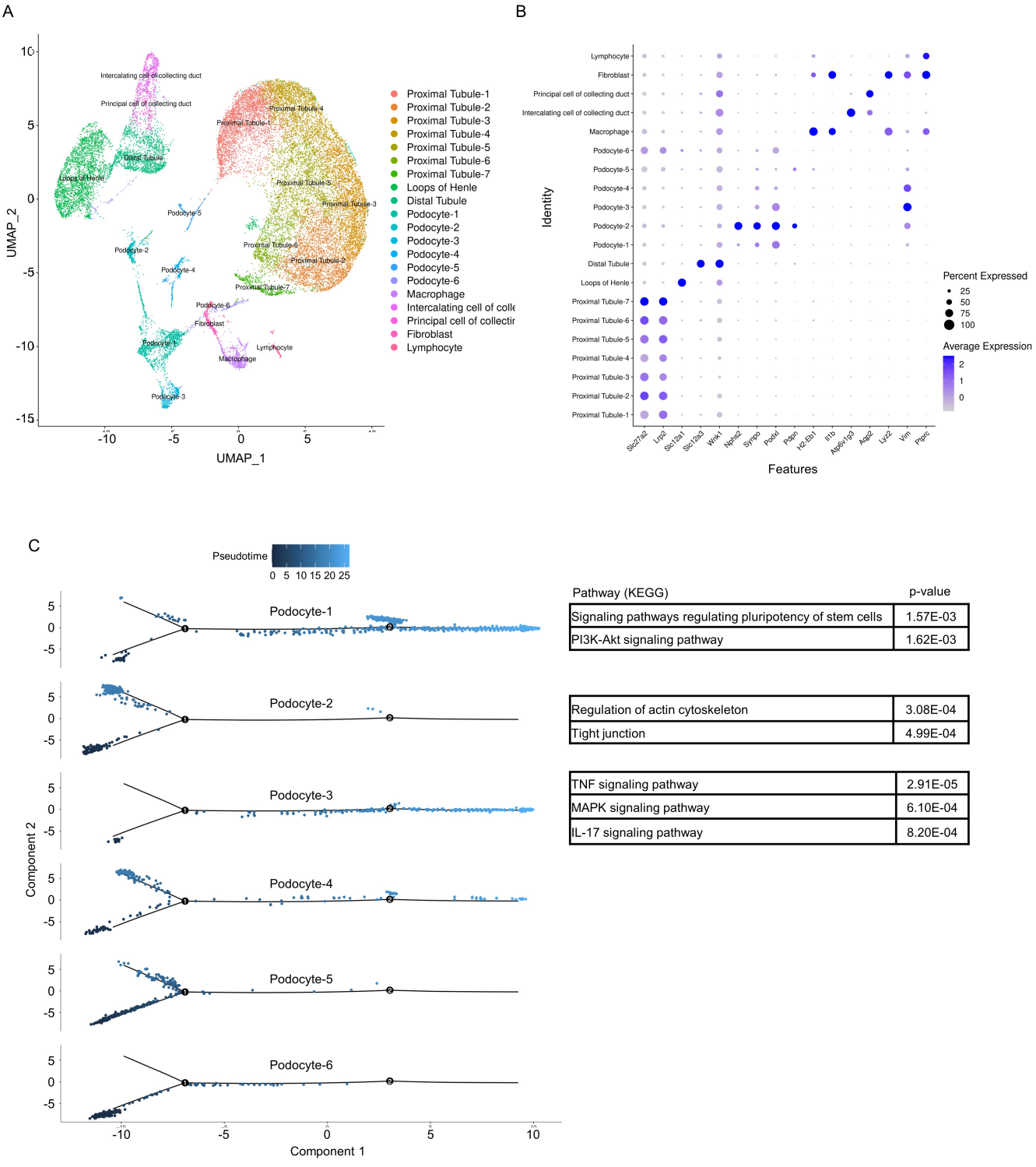

Pathway (KEGG)	p-value
Signaling pathways regulating pluripotency of stem cells	1.57E-03
PI3K-Akt signaling pathway	1.62E-03
Regulation of actin cytoskeleton	3.08E-04
Tight junction	4.99E-04
TNF signaling pathway	2.91E-05
MAPK signaling pathway	6.10E-04
IL-17 signaling pathway	8.20E-04

Figure 2

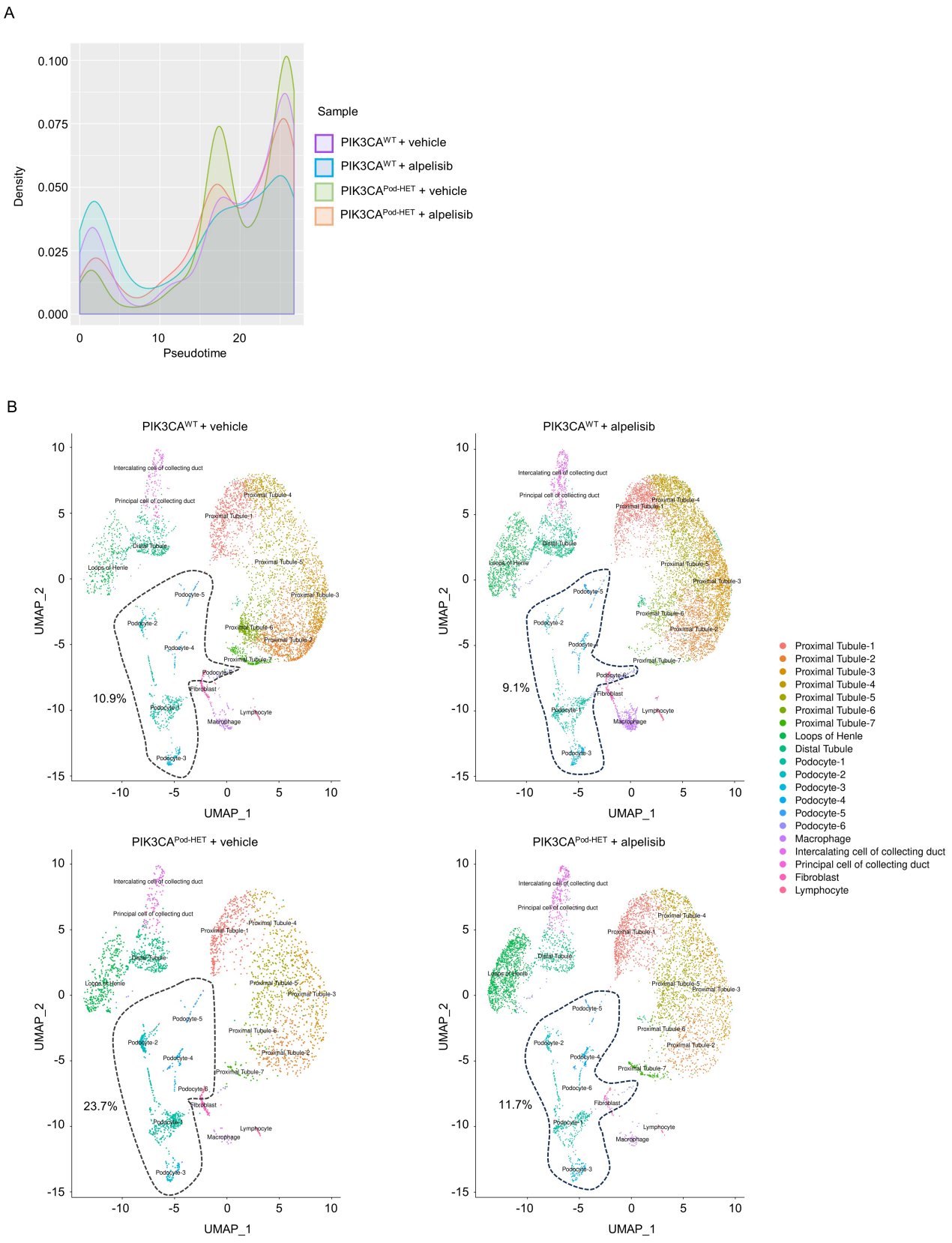
A
Density
Pseudotime
Sample
PIK3CA^WT + vehicle
PIK3CA^WT + alpelisib
PIK3CA^Pod-HET + vehicle
PIK3CA^Pod-HET + alpelisib
B
PIK3CA^WT + vehicle
PIK3CA^WT + alpelisib
PIK3CA^Pod-HET + vehicle
PIK3CA^Pod-HET + alpelisib
UMAP_1
UMAP_2
10.9%
9.1%
23.7%
11.7%
Proximal Tubule-1
Proximal Tubule-2
Proximal Tubule-3
Proximal Tubule-4
Proximal Tubule-5
Proximal Tubule-6
Proximal Tubule-7
Loops of Henle
Distal Tubule
Podocyte-1
Podocyte-2
Podocyte-3
Podocyte-4
Podocyte-5
Podocyte-6
Macrophage
Intercalating cell of collecting duct
Principal cell of collecting duct
Fibroblast
Lymphocyte

Figure 3

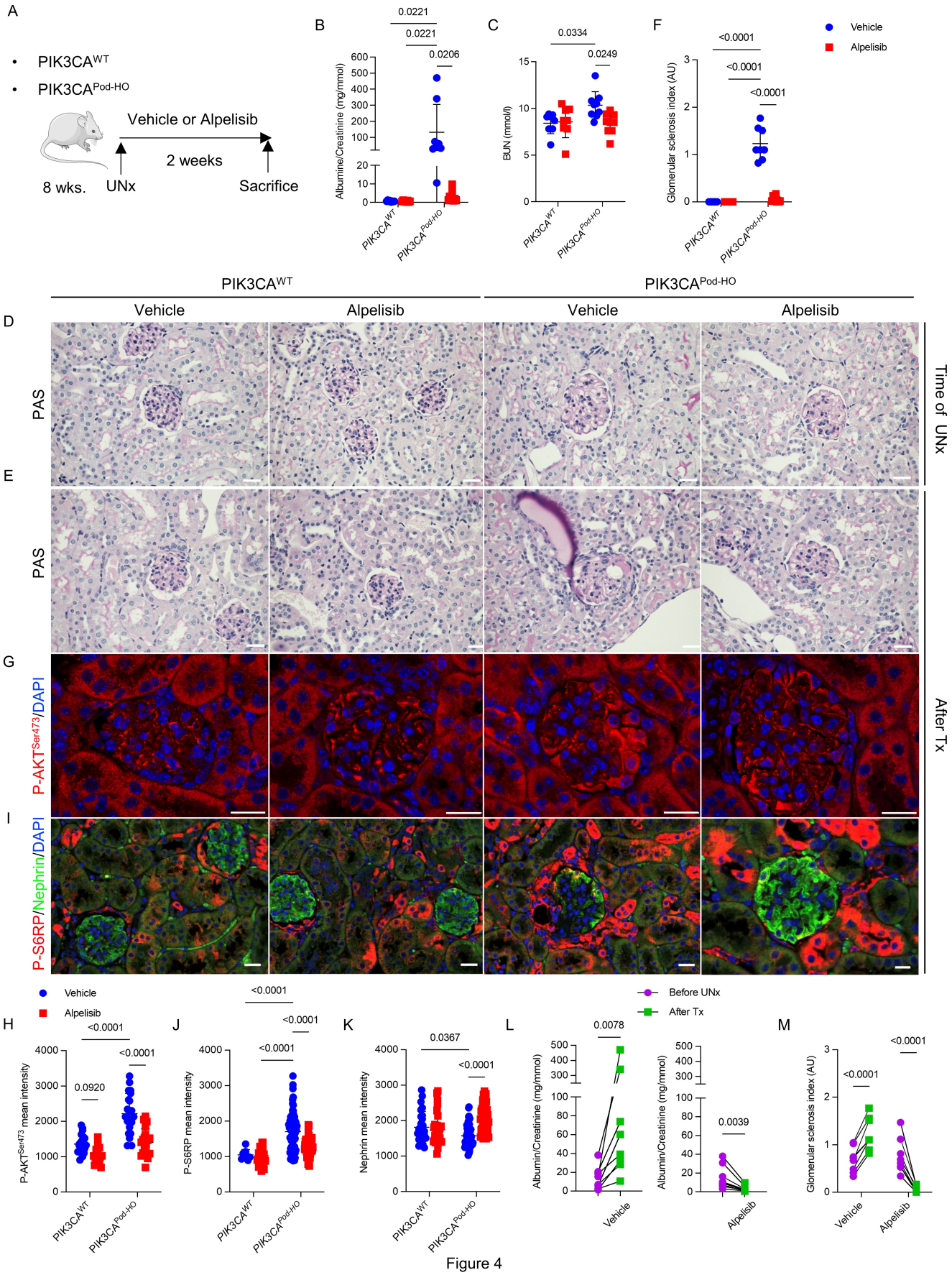
A
PIK3CA^WT
PIK3CA^Pod-HO
Vehicle or Alpelisib
2 weeks
8 wks.
UNx
Sacrifice
B
Albumine/Creatinine (mg/mmol)
0.0221
0.0221
0.0206
C
BUN (mmol/l)
0.0334
0.0249
F
Glomerular sclerosis index (AU)
<0.0001
<0.0001
<0.0001
Vehicle
Alpelisib
PIK3CA^WT
PIK3CA^Pod-HO
Vehicle
Alpelisib
Vehicle
Alpelisib
D
PAS
E
PAS
Time of UNx
G
P-AKT^Ser473/DAPI
I
P-S6RP/Nephrin/DAPI
After Tx
Vehicle
Alpelisib
H
P-AKT^Ser473 mean intensity
<0.0001
<0.0001
0.0920
J
P-S6RP mean intensity
<0.0001
<0.0001
<0.0001
K
Nephrin mean intensity
0.0367
<0.0001
Before UNx
After Tx
L
Albumin/Creatinine (mg/mmol)
0.0078
0.0039
Vehicle
Alpelisib
M
Glomerular sclerosis index (AU)
<0.0001
<0.0001
Vehicle
Alpelisib

Figure 4

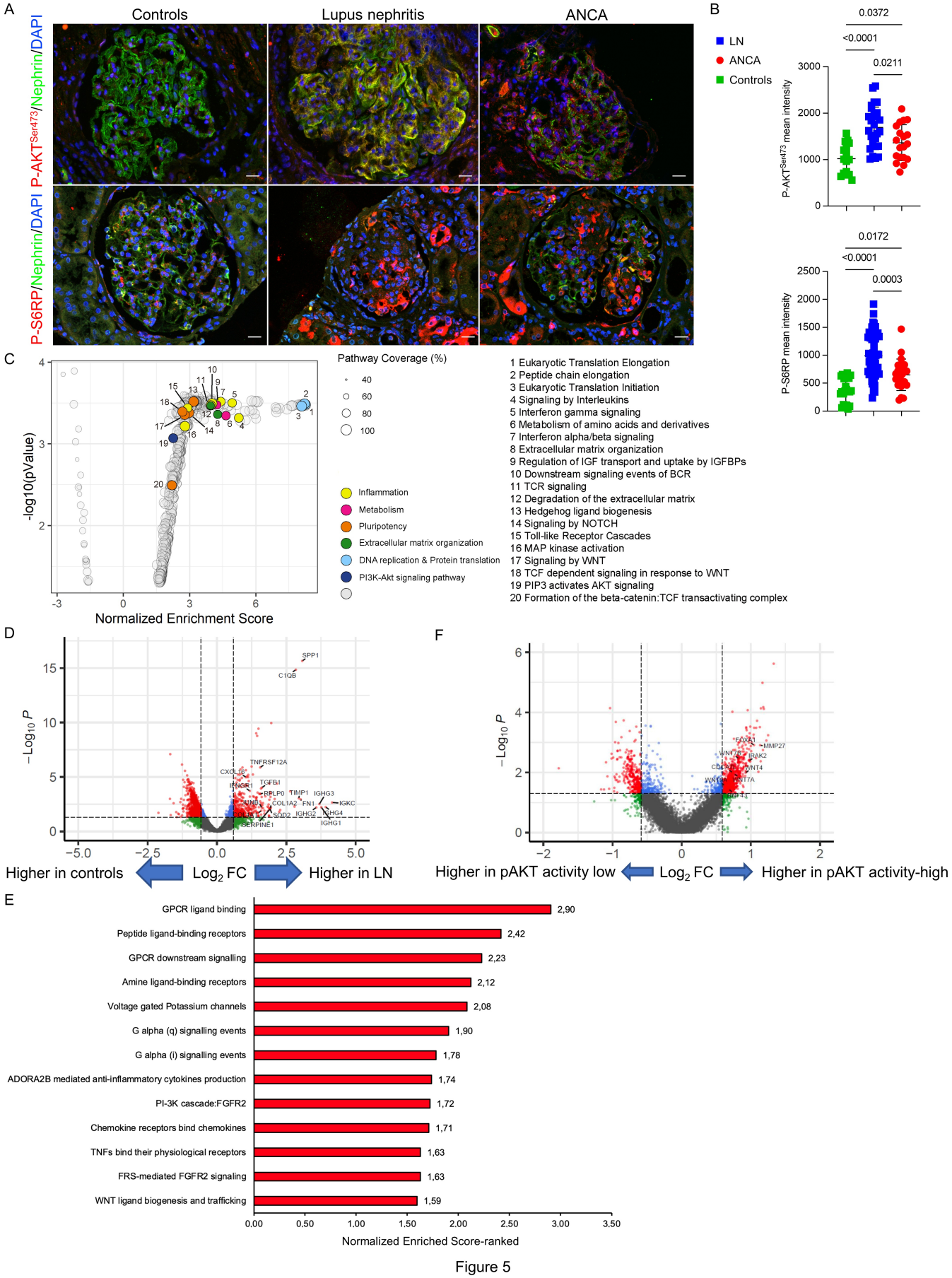
A
Controls
Lupus nephritis
ANCA
P-AKTSer473/Nephrin/DAPI
P-S6RP/Nephrin/DAPI
B
LN
ANCA
Controls
0.0372
<0.0001
0.0211
P-AKTSer473 mean intensity
0.0172
<0.0001
0.0003
P-S6RP mean intensity
C
-log10(pValue)
Normalized Enrichment Score
Pathway Coverage (%)
40
60
80
100
Inflammation
Metabolism
Pluripotency
Extracellular matrix organization
DNA replication & Protein translation
PI3K-Akt signaling pathway
1 Eukaryotic Translation Elongation
2 Peptide chain elongation
3 Eukaryotic Translation Initiation
4 Signaling by Interleukins
5 Interferon gamma signaling
6 Metabolism of amino acids and derivatives
7 Interferon alpha/beta signaling
8 Extracellular matrix organization
9 Regulation of IGF transport and uptake by IGFBPs
10 Downstream signaling events of BCR
11 TCR signaling
12 Degradation of the extracellular matrix
13 Hedgehog ligand biogenesis
14 Signaling by NOTCH
15 Toll-like Receptor Cascades
16 MAP kinase activation
17 Signaling by WNT
18 TCF dependent signaling in response to WNT
19 PIP3 activates AKT signaling
20 Formation of the beta-catenin:TCF transactivating complex
D
−Log10 P
SPP1
C1QB
TNFRSF12A
CXCL12
TGFB1
IFNGR1
RPLP0
TIMP1
IGHG3
COL1A2
FN1
IGKC
SPARC
SOD2
IGHG2
IGHG4
IGHG1
SERPINE1
Higher in controls
Log2 FC
Higher in LN
F
−Log10 P
FOXA1
MMP27
IRAK2
WNT4
WNT7A
CDH1
WNT10A
KRT7A
Higher in pAKT activity low
Log2 FC
Higher in pAKT activity-high
E
GPCR ligand binding 2,90
Peptide ligand-binding receptors 2,42
GPCR downstream signalling 2,23
Amine ligand-binding receptors 2,12
Voltage gated Potassium channels 2,08
G alpha (q) signalling events 1,90
G alpha (i) signalling events 1,78
ADORA2B mediated anti-inflammatory cytokines production 1,74
PI-3K cascade:FGFR2 1,72
Chemokine receptors bind chemokines 1,71
TNFs bind their physiological receptors 1,63
FRS-mediated FGFR2 signaling 1,63
WNT ligand biogenesis and trafficking 1,59
Normalized Enriched Score-ranked

Figure 5

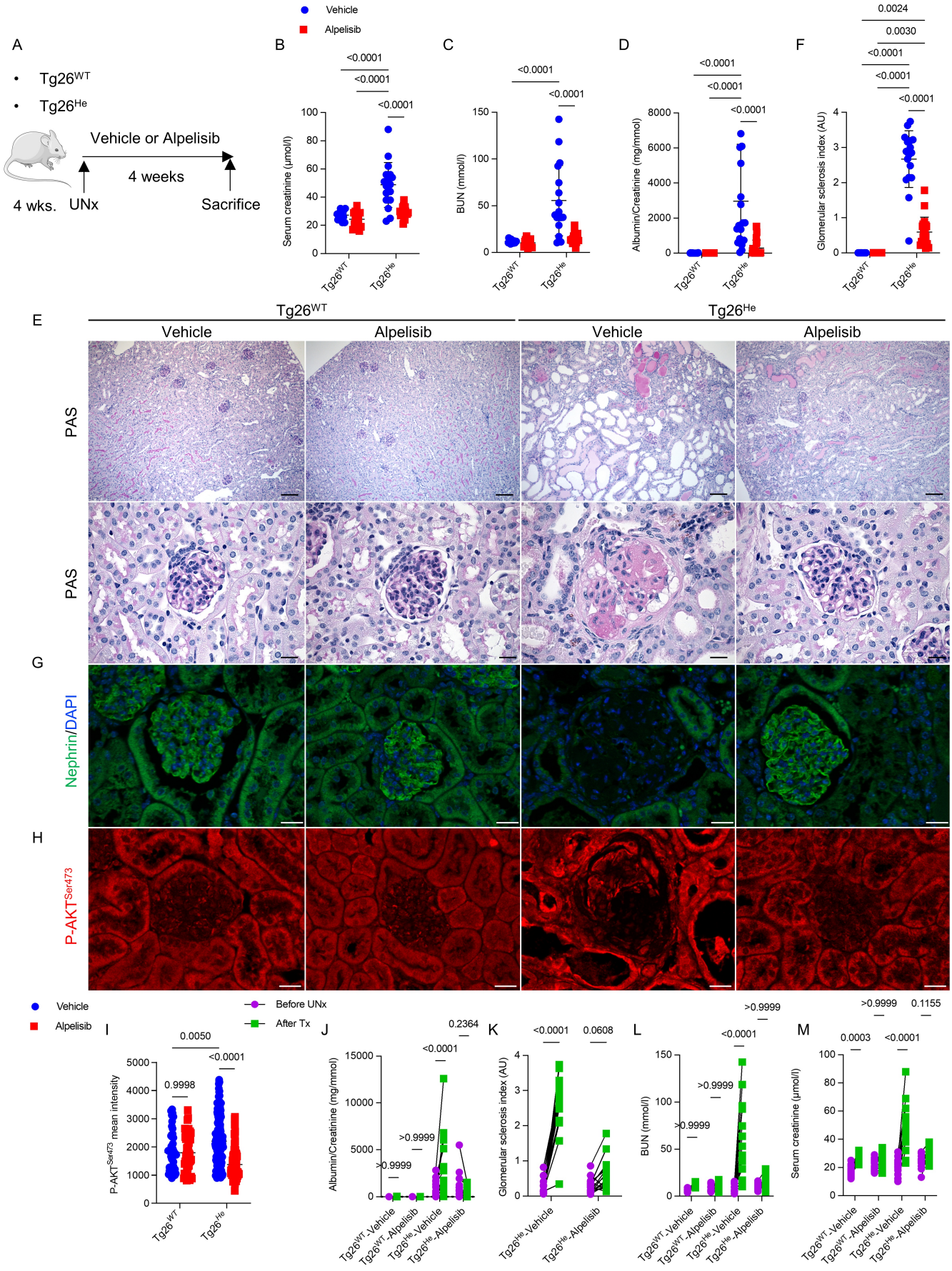
A
Tg26WT
Tg26He
Vehicle or Alpelisib
4 weeks
4 wks.
UNx
Sacrifice
B
Vehicle
Alpelisib
Serum creatinine (μmol/l)
C
BUN (mmol/l)
D
Albumin/Creatinine (mg/mmol)
F
Glomerular sclerosis index (AU)
E
Tg26WT
Tg26He
Vehicle
Alpelisib
PAS
G
Nephrin/DAPI
H
P-AKTSer473
Before UNx
After Tx
I
P-AKTSer473 mean intensity
J
K
L
M

Figure 6

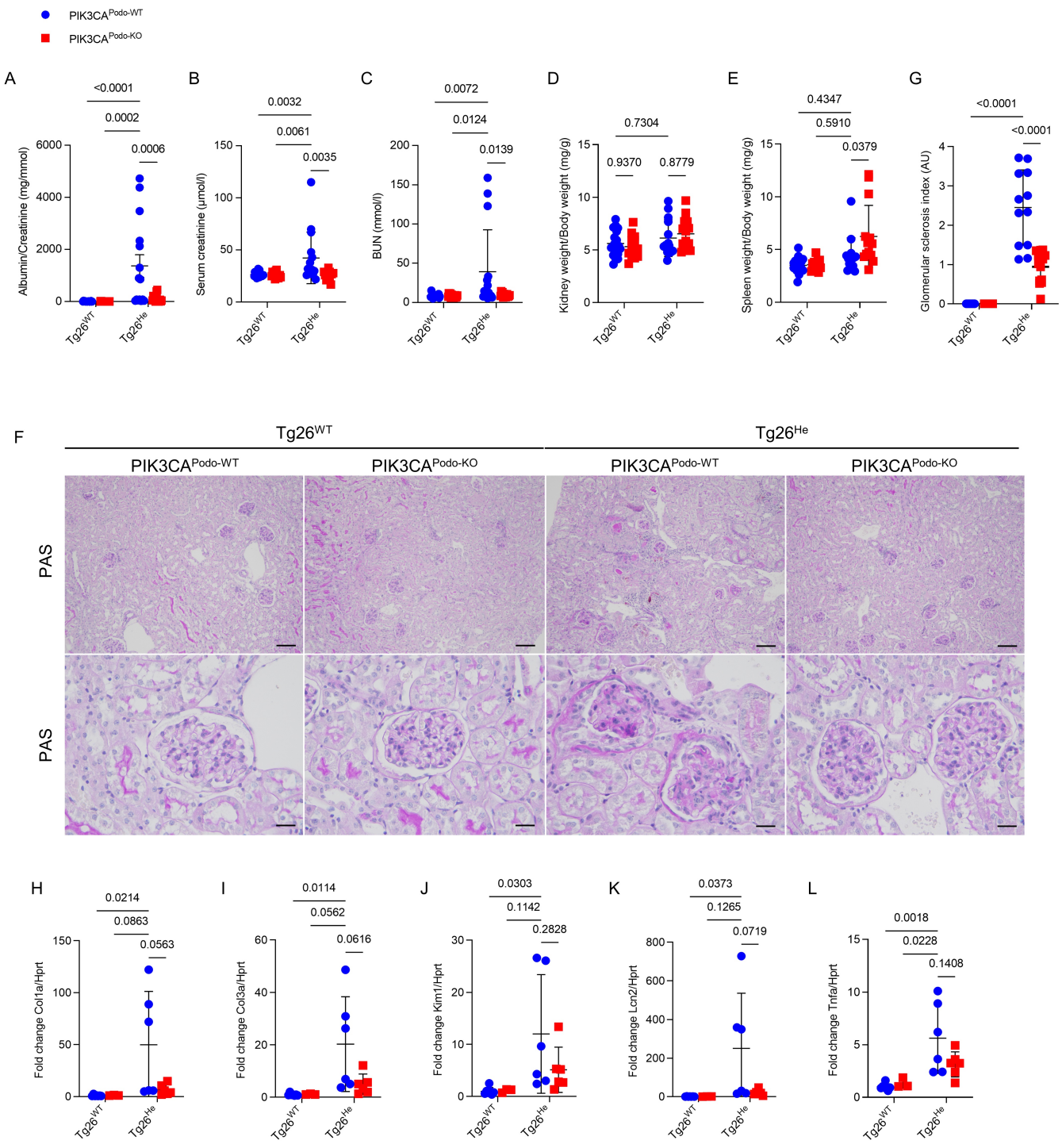
PIK3CA Podo-WT
PIK3CA Podo-KO
A
<0.0001
0.0002
0.0006
Albumin/Creatinine (mg/mmol)
B
0.0032
0.0061
0.0035
Serum creatinine (μmol/l)
C
0.0072
0.0124
0.0139
BUN (mmol/l)
D
0.7304
0.9370
0.8779
Kidney weight/Body weight (mg/g)
E
0.4347
0.5910
0.0379
Spleen weight/Body weight (mg/g)
G
<0.0001
<0.0001
Glomerular sclerosis index (AU)
Tg26WT
Tg26He
F
Tg26WT
Tg26He
PIK3CA Podo-WT
PIK3CA Podo-KO
PAS
H
0.0214
0.0863
0.0563
Fold change Col1a/Hprt
I
0.0114
0.0562
0.0616
Fold change Col3a/Hprt
J
0.0303
0.1142
0.2828
Fold change Kim1/Hprt
K
0.0373
0.1265
0.0719
Fold change Lcn2/Hprt
L
0.0018
0.0228
0.1408
Fold change Tnfa/Hprt

Figure 7

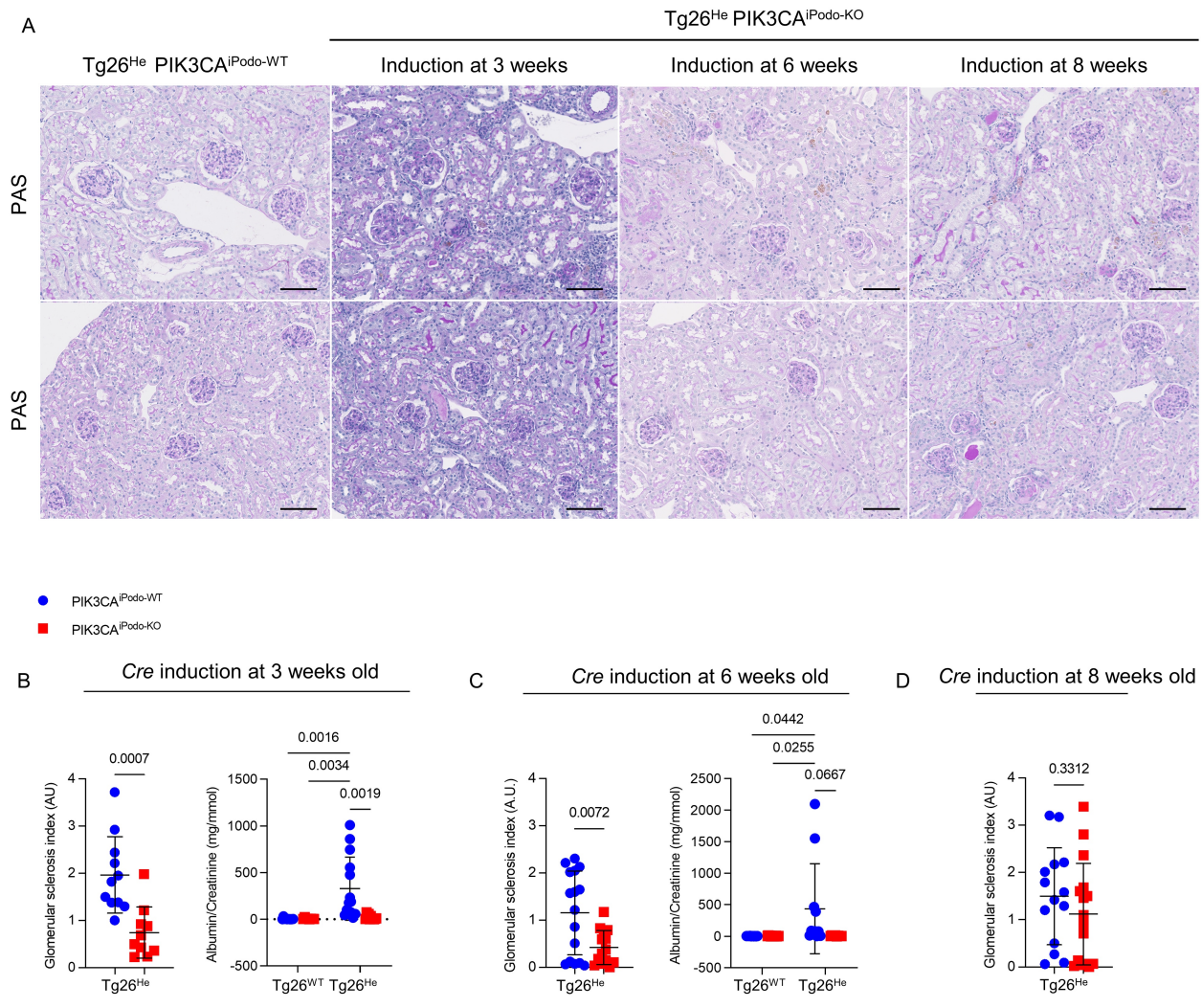
A
Tg26He PIK3CAiPodo-KO
Tg26He PIK3CAiPodo-WT
Induction at 3 weeks
Induction at 6 weeks
Induction at 8 weeks
PAS
PAS
PIK3CAiPodo-WT
PIK3CAiPodo-KO
B
Cre induction at 3 weeks old
Glomerular sclerosis index (AU)
0.0007
Tg26He
Albumin/Creatinine (mg/mmol)
0.0016
0.0034
0.0019
Tg26WT
Tg26He
C
Cre induction at 6 weeks old
Glomerular sclerosis index (A.U.)
0.0072
Tg26He
Albumin/Creatinine (mg/mmol)
0.0442
0.0255
0.0667
Tg26WT
Tg26He
D
Cre induction at 8 weeks old
Glomerular sclerosis index (AU)
0.3312
Tg26He

Figure 8

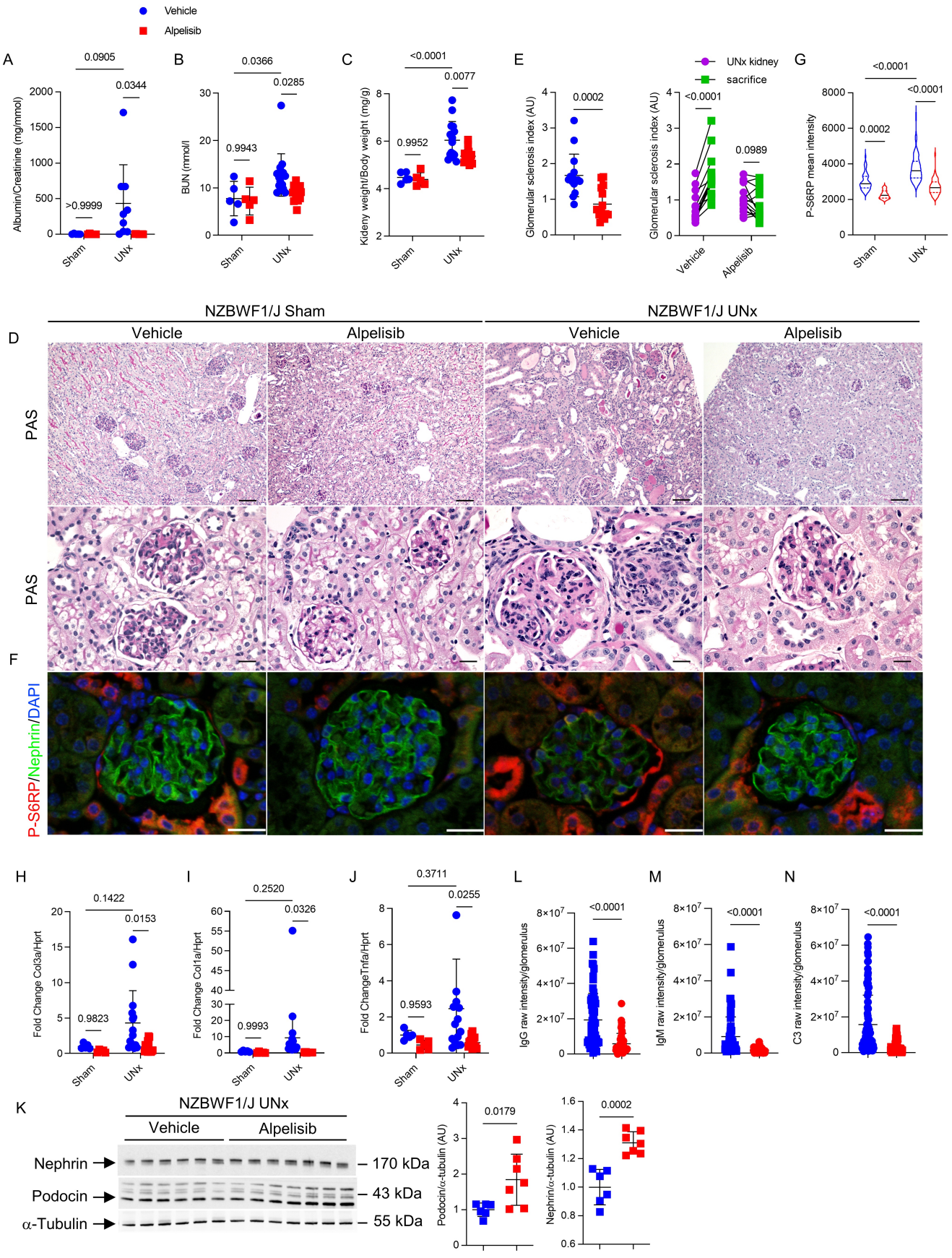
Vehicle
Alpelisib
A
Albumin/Creatinine (mg/mmol)
0.0905
0.0344
>0.9999
Sham
UNx
B
BUN (mmol/l
0.0366
0.0285
0.9943
C
Kideny weight/Body weight (mg/g)
<0.0001
0.0077
0.9952
E
Glomerular sclerosis index (AU)
0.0002
UNx kidney
sacrifice
<0.0001
0.0989
Vehicle
Alpelisib
G
P-S6RP mean intensity
<0.0001
<0.0001
0.0002
NZBWF1/J Sham
NZBWF1/J UNx
D
PAS
F
P-S6RP/Nephrin/DAPI
H
Fold Change Col3a/Hprt
0.1422
0.0153
0.9823
I
Fold Change Col1a/Hprt
0.2520
0.0326
0.9993
J
Fold ChangeTnfa/Hprt
0.3711
0.0255
0.9593
L
IgG raw intensity/glomerulus
<0.0001
M
IgM raw intensity/glomerulus
<0.0001
N
C3 raw intensity/glomerulus
<0.0001
K
NZBWF1/J UNx
Nephrin
Podocin
α-Tubulin
170 kDa
43 kDa
55 kDa
Podocin/α-tubulin (AU)
0.0179
Nephrin/α-tubulin (AU)
0.0002

Figure 9

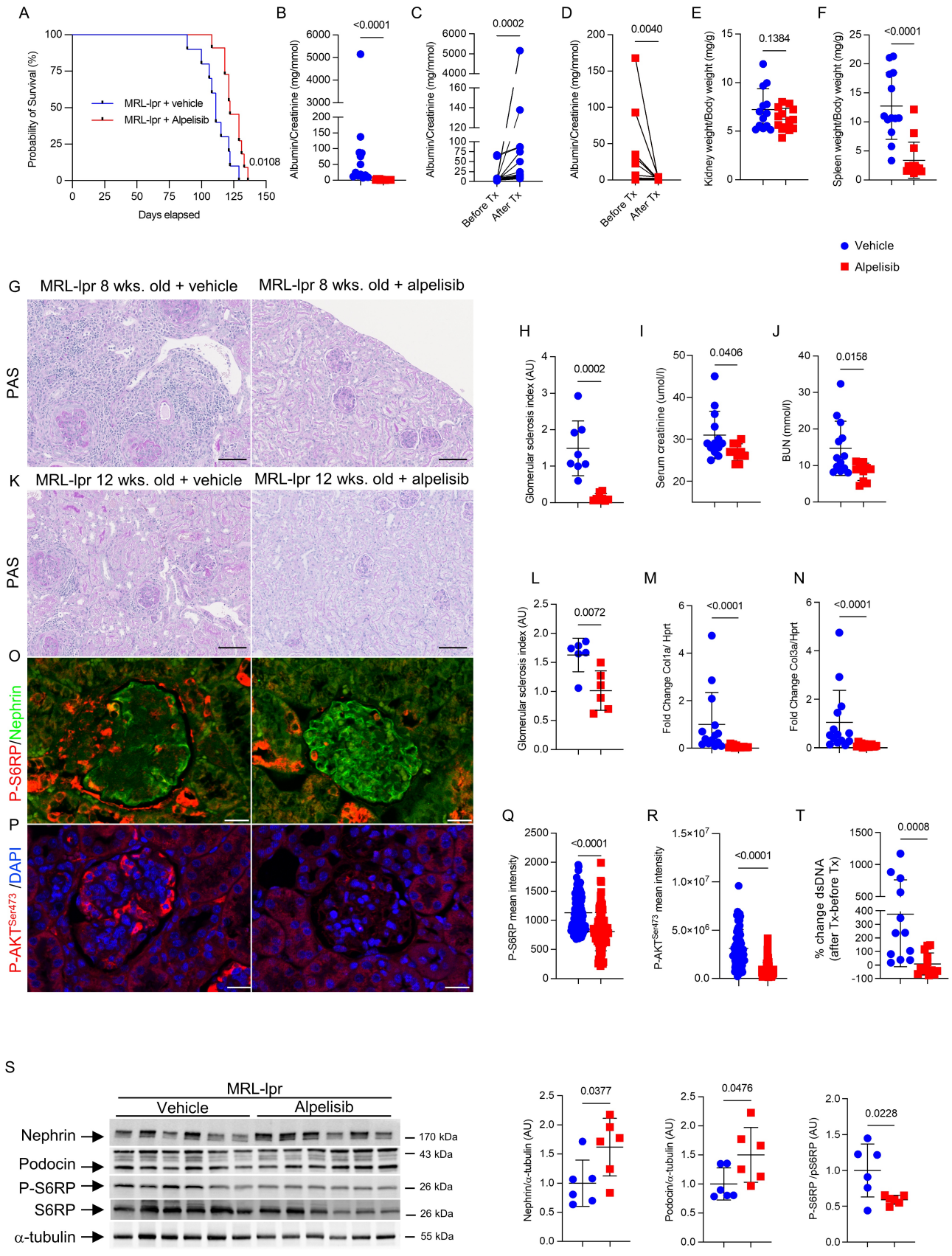
A
Probability of Survival (%)
MRL-lpr + vehicle
MRL-lpr + Alpelisib
0.0108
Days elapsed
B
Albumin/Creatinine (mg/mmol)
<0.0001
C
Albumin/Creatinine (mg/mmol)
0.0002
Before Tx
After Tx
D
Albumin/Creatinine (mg/mmol)
0.0040
Before Tx
After Tx
E
Kidney weight/Body weight (mg/g)
0.1384
F
Spleen weight/Body weight (mg/g)
<0.0001
Vehicle
Alpelisib
G
MRL-lpr 8 wks. old + vehicle
MRL-lpr 8 wks. old + alpelisib
PAS
H
Glomerular sclerosis index (AU)
0.0002
I
Serum creatinine (umol/l)
0.0406
J
BUN (mmol/l)
0.0158
K
MRL-lpr 12 wks. old + vehicle
MRL-lpr 12 wks. old + alpelisib
PAS
L
Glomerular sclerosis index (AU)
0.0072
M
Fold Change Col1a1/ Hprt
<0.0001
N
Fold Change Col3a/Hprt
<0.0001
O
P-S6RP/Nephrin
P
P-AKTSer473 /DAPI
Q
P-S6RP mean intensity
<0.0001
R
P-AKTSer473 mean intensity
<0.0001
T
% change dsDNA (after Tx-before Tx)
0.0008
S
MRL-lpr
Vehicle
Alpelisib
Nephrin
Podocin
P-S6RP
S6RP
α-tubulin
170 kDa
43 kDa
26 kDa
26 kDa
55 kDa
Nephrin/α-tubulin (AU)
0.0377
Podocin/α-tubulin (AU)
0.0476
P-S6RP /pS6RP (AU)
0.0228

Figure 10

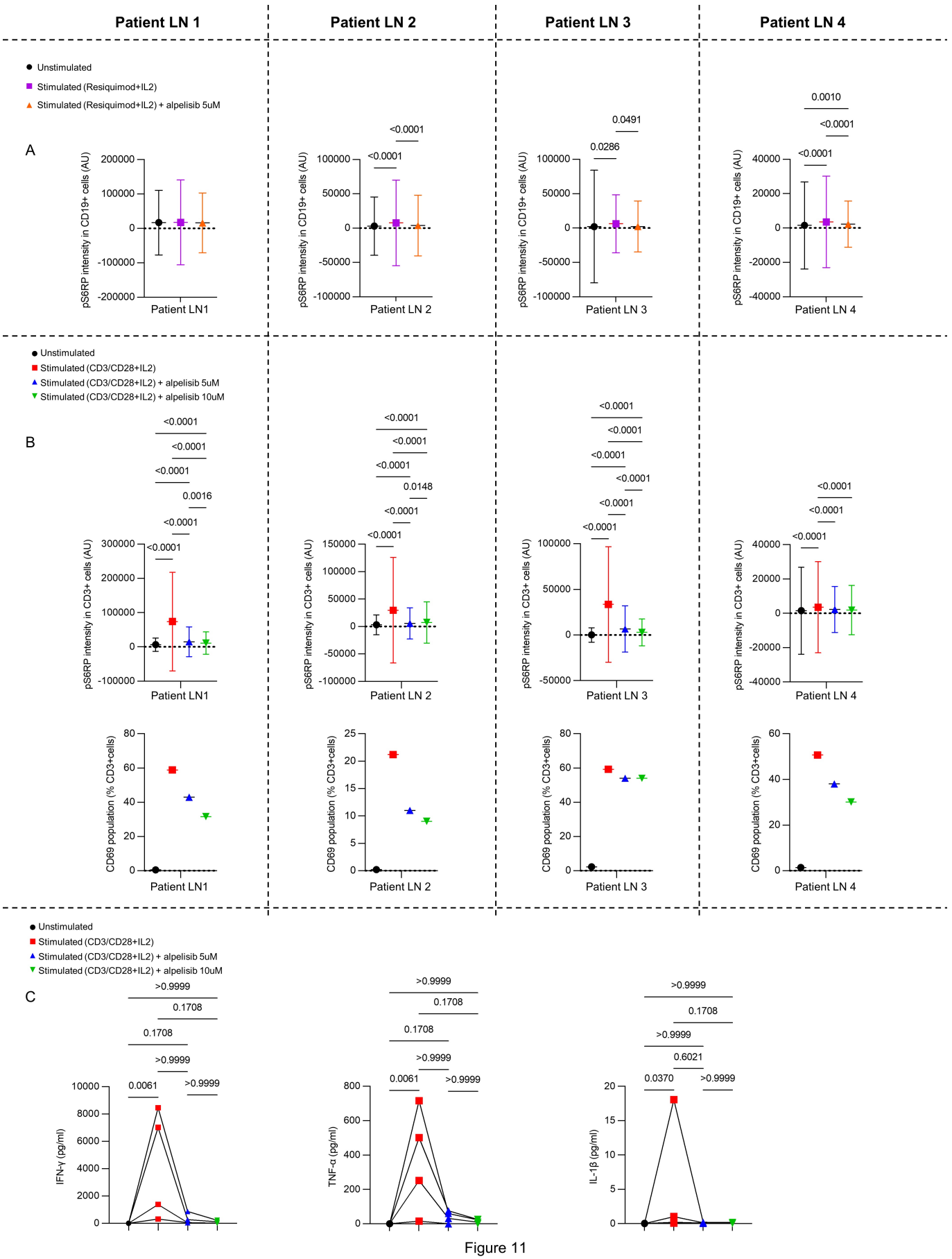
Patient LN 1
Patient LN 2
Patient LN 3
Patient LN 4
Unstimulated
Stimulated (Resiquimod+IL2)
Stimulated (Resiquimod+IL2) + alpelisib 5uM
A
pS6RP intensity in CD19+ cells (AU)
Patient LN1
Patient LN 2
Patient LN 3
Patient LN 4
Unstimulated
Stimulated (CD3/CD28+IL2)
Stimulated (CD3/CD28+IL2) + alpelisib 5uM
Stimulated (CD3/CD28+IL2) + alpelisib 10uM
B
pS6RP intensity in CD3+ cells (AU)
CD69 population (% CD3+cells)
Patient LN1
Patient LN 2
Patient LN 3
Patient LN 4
Unstimulated
Stimulated (CD3/CD28+IL2)
Stimulated (CD3/CD28+IL2) + alpelisib 5uM
Stimulated (CD3/CD28+IL2) + alpelisib 10uM
C
IFN-γ (pg/ml)
TNF-α (pg/ml)
IL-1β (pg/ml)

Figure 11